Temperature- and Pressure-Dependent Kinetics of CH2OO + CH3COCH3 and CH2OO + CH3CHO: Direct Measurements and Theoretical Analysis

Temperature and Pressure Dependent Kinetics of $CH_2OO + CH_3COCH_3$ and $CH_2OO + CH_3CHO$: Direct Measurements and Theoretical Analysis

Rehab M. I. Elsamra,[†,‡] Amrit Jalan,[†] Zachary J. Buras,[†] Joshua E. Middaugh,[†] and William H. Green.[†*]

[†]Department of Chemical Engineering, Massachusetts Institute of Technology, 77 Massachusetts Avenue, Cambridge, MA 02139, USA.

[‡]Department of Chemistry, Faculty of Science, Alexandria University, Ibrahimia, 21321, Alexandria, Egypt.

The rate coefficients of the gas-phase reactions $CH_2OO + CH_3COCH_3$ and $CH_2OO + CH_3CHO$ have been experimentally determined from 298 - 500 K and 4 – 50 torr using pulsed laser photolysis with multiple-pass UV absorption at 375 nm, and products were detected using photoionization mass spectrometry at 10.5 eV. The $CH_2OO + CH_3CHO$ reaction's rate coefficient is ~4 times faster over the temperature 298-500 K range studied here. Both reactions have negative temperature dependence. The *T*-dependence of both reactions was captured in simple Arrhenius expressions:

$k_{CH2OO+CH3COCH3}(T) = (7 \pm 2.5) \times 10^{-15}$ cm^3 molecule^{-1} s^{-1} exp[+(9.3 ±2.9) kJ mol^{-1}/RT]
$k_{CH2OO+CH3CHO}(T) = (3 \pm 0.8) \times 10^{-14}$ cm^3 molecule^{-1} s^{-1} exp[+(9.1 ±2.7) kJ mol^{-1}/RT]

The rate of the reactions of CH_2OO with carbonyl compounds at room temperature is two orders of magnitude higher than that reported previously for the reaction with alkenes, but the A factors are of the same order of magnitude. Theoretical analysis of the entrance channel reveals that the inner 1,3-cycloaddition transition state is rate-limiting at normal temperatures. Predicted rate-coefficients (RCCSD(T)-F12a/cc-pVTZ-F12//B3LYP/MG3S level of theory) in the low-pressure limit accurately reproduce the experimentally observed temperature dependence. The calculations only qualitatively reproduce the A factors and the relative reactivity between CH_3CHO and CH_3COCH_3. The rate coefficients are weakly pressure-dependent, within the uncertainties of the current measurements. The predicted major products are not detectable with our photo-ionization source, but heavier species yielding ions with masses m/z = 104 and m/z = 89 are observed as products from the reaction of CH_2OO with CH_3COCH_3. The yield of m/z = 89 exhibits positive pressure dependence that appears to have already reached a high-pressure limit by 25 Torr.

Keywords: Criegee intermediate, Carbonyl compounds, multi-pass laser absorption, absolute rate constants, temperature dependence, pressure dependence, relative product branching, master equation calculation

1. Introduction

Criegee Intermediates (CI) were postulated many years ago as important biradicals in atmospheric alkene ozonolysis[1] where they are likely to be formed with high internal energy and can initiate tropospheric oxidation reactions.[2] They also impact the atmospheric budgets of SO_2[3] and NO_X[4,5] and are linked to the formation of H_2SO_4.[6] Reaction of CI with water dimer is by far the major bimolecular loss for this intermediate, which is based on the high concentration of H_2O in the troposphere and the moderate rate constant of the reaction of CI with water dimer.[7] For its potential importance in the atmosphere, reactions of CI with neutral atmospheric molecules have been of interest to many experimentalists and theoreticians.[2-11] However, direct kinetic measurements were only accessible recently, after Welz *et al.* demonstrated an efficient route for the formation of the simplest CI (CH_2OO) through the reaction of $CH_2I + O_2$.[4] Reactions with carbonyl compounds have received special attention as the highly exothermic and barrierless cycloaddition of CI to the C=O bond makes them efficient CI scavengers. In the present work, we report the temperature dependent rate coefficients for reactions of CH_2OO with CH_3COCH_3 and CH_3CHO and compare these with similar studies on C2-C4 alkenes (ethene, propene and butenes).[8] Existing literature on the carbonyl reactions has been limited to room temperature.[9-13] Taatjes *et al.*[9] used Photo-Ionization Mass Spectrometry (PIMS) and found the reaction with CH_3CHO to be 4 times faster than with CH_3COCH_3 at P = 4 Torr. In the case of CH_3COCH_3 they observed products at two masses: m/z =104 amu, which they assigned to the secondary ozonide (SOZ) and m/z = 89 amu, which they hypothesized was the daughter ion of another 104 amu isomer. Acetic acid (CH_3COOH), formaldehyde (HCHO) and formic acid (HCOOH) were all detected as products in the reaction between CH_2OO and CH_3CHO. Stone *et al.*[10] investigated the reaction of CH_2OO with CH_3CHO at pressures between 25 Torr and 300 Torr. They monitored HCHO and found the HCHO yield from the reaction to decrease with pressure, implying that the reaction is pressure dependent. Horie *et al.*[11] used FT-IR to measure the rate of CH_2OO reaction with CH_3CHO relative to CF_3COCF_3 in the solution phase and observed SOZ formation in both reactions. Berndt *et al.* [12] measured the room temperature rate coefficient for the reactions of CH_2OO with CH_3CHO and CH_3COCH_3. In their work, CH_2OO radicals were generated from the reaction of ozone with C_2H_4 at atmospheric pressure and the rate coefficient was indirectly measured by detecting H_2SO_4 after titration with SO_2. Several *ab initio* calculations have been performed on CH_2OO + carbonyls.[13-15] Recently Jalan *et al.*[15] used electronic structure and RRKM calculations to determine both the rates and the product branching of the

title reactions. Buras *et al.* reported rates for reactions of CH_2OO with alkenes[8] and found the kinetics to be slow relative to carbonyl compounds with small positive experimental *E*a's. The main interest of this article is to measure and understand the *T*-dependence of CH_2OO + C=O bonds in CH_3CHO and CH_3COCH_3 and compare these with similar results for CH_2OO + C=C bonds obtained earlier. We also report the effect of pressure on the kinetics of the title reactions at 298 K and 444 K. The products of the reactions were measured at 298 K and 10, 25 and 50 Torr by Photo-Ionization Time-of-Flight Mass Spectrometry (PI TOF-MS). The MS study was limited to products with ionization energy ≤ 10.5 eV. Finally, our measurements were compared against theoretical predictions using the molecular geometries and energies computed by Jalan *et al.* (RCCSD(T)-F12a/cc-pVTZ-F12//B3LYP/MG3S level of theory).[15]

2. Experimental Methods

All experiments were conducted on a modified version of the MIT laser-photolysis/Herriott multiple-pass laser-absorption apparatus described by Ismail *et al.*[16] This apparatus was modified to incorporate a PI TOF-MS with supersonic molecular beam sampling from the center of the reactor. Detailed descriptions of the apparatus are available in a published MIT Ph.D. thesis[17] and only the essential details are included here. The stainless steel reactor is 86 cm long, 6 cm in diameter and resistively heated by four heaters wrapped along the length of the reactor to create a uniform temperature profile (standard deviation ±2% of average) through the overlap region of the absorption laser. The heaters enable the gas mixture to be heated up to 700 K, though in the present work, measurements were limited to 500 K to avoid secondary chemistry that could arise from the thermal decomposition of CH_2OO at high temperatures. The internal pressure of the reactor was monitored by a capacitance manometer and controlled *via* an automated butterfly valve. In order to minimize the possibility of CH_2 formation (*via* a single-photon process[18]) or photolytic fragmentation of either CH_3CHO or CH_3COCH_3, the third harmonic output of a Nd:YAG laser (355 nm) operated at a repetition rate of 2 Hz was used to photolyze CH_2I_2 instead of a shorter wavelength such as the fourth harmonic of a Nd:YAG laser (266 nm). The frequency-doubled output of a Ti:Sapphire laser (80 MHz pulsed laser with 1.2 ps full width at half maximum, FWHM, pulses) was used to generate the 375 nm probe beam. The fundamental wavelength of the Ti:Sapphire laser was measured before each experiment using a recently calibrated Ocean Optics USB2000 spectrometer. Multiple-pass probe laser path lengths were in the range of 10−15 m.

Because the probe laser generates a continuous pulse train, a complete transient absorption trace is recorded for each photolysis flash. Transient absorbance traces were averaged over 500 acquisitions. Helium was used as a balance gas. The flow of this gas was varied to adjust the total gas mixture flow and maintain the same number of photolysis flashes per refresh. All experiments were operated at one flash per refresh to avoid secondary chemistry.

The relative time-dependent product concentrations were determined using the PI TOF-MS method. A small amount of the reactive gas mixture was continuously sampled *via* a small pinhole at the tip of a cone that juts slightly into cross section of the photolysis beam at the center of the reaction cell. The sampled gas was supersonically expanded, and the center of the resultant free jet was passed through a Beam Dynamics skimmer to form a collimated molecular beam. The gas in the molecular beam was effectively "frozen" in composition by cooling while in transit to the ionization region of the PI TOF-MS, where it was photo-ionized using 118.2 nm (10.487 eV) light. The 118.2 nm light was generated by focusing the third harmonic (355 nm) output of a pulsed Nd:YAG laser (<12 ns FWHM wide pulses at 2Hz) in a 1:10 Xe:Ar gas cell at a total pressure of 90–100 Torr. The relative abundance of ions at different mass-to-charge ratios (m/z) were analyzed using a Kore Time-of-Flight mass spectrometer and detected using the Kore-supplied discrete dynode electron multiplier detector and analog pre-amplifier. The correspondence between time-of-flight and m/z was determined by calibration with a mixture of known stable species. Control experiments were conducted with and without acetone, O_2 or CH_2I_2.

CH_2I_2 was purchased from Sigma-Aldrich at 99% purity and was further purified by successive freeze-pump-thaw cycles. CH_2I_2 was introduced into the reactor by a helium flow through a room temperature bubbler maintained at 750 Torr. CH_3COCH_3 (Sigma Aldrich, ≥ 99.9%) and CH_3CHO (Sigma Aldrich, ≥ 99.5%) were used after purification by freeze-pump-thaw cycles using liquid nitrogen. During use, the carbonyl compounds were maintained at constant temperatures such that their respective vapor pressures were sufficient to drive the flow through an MKS mass flow controller (MFC). Because the MFC's have been calibrated with N_2, the uncertainty in the concentration of CH_3CHO and CH_3COCH_3 in the reactor is 10%, as we have previously explained,[8] which is the dominant contribution to the uncertainty in our measurements of overall rate coefficients. In the TOF-MS experiments a small flow of calibration gas, consisting of 100 ppm each of nine species with known

photoionization cross sections diluted in helium, was simultaneously introduced as an internal standard. The uncertainty in the concentration of the calibration gas is also 10% for the same reasons, which has been accounted for in the final reported uncertainty of our TOF-MS results. Helium (Airgas, 99.999%) and oxygen (BOC, 99.999%) were used directly without further purification.

3. Results and discussion

3.1 Generation of CH_2OO

CH_2OO radicals were generated utilizing the method demonstrated by Welz *et al.*, (but using 355 nm instead of 248 nm photolysis) [4]

$$CH_2I_2 \xrightarrow{355\ nm} CH_2I + I$$

$$CH_2I + O_2 \xrightarrow{k_1} CH_2OO + I$$

Figure 1 shows the CH_2OO absorption signals of the 375 nm photons from the Ti:Sapphire probe beam following the 355 nm photolysis of CH_2I_2 in the presence of O_2. Flat signal was observed in the absence of either CH_2I_2 or O_2. Previous work in our laboratory[8] has demonstrated that CH_2OO was the radical being probed in our apparatus at 375 nm. Verification was by following the formation rate of CH_2OO by simultaneously recording the UV absorption at 375 nm and the infrared absorption of the co-product I atoms atomic transition (F= 3 $^2P_{1/2}$ ← F=4 $^2P_{3/2}$)[18] at different concentrations of O_2. The resulting rate coefficient (k_1) agrees well with literature confirming that the species being monitored is a product of $CH_2I + O_2$. Furthermore, the room temperature reaction rate of this species with CH_3COCH_3 agrees well with Taatjes's value[9] for $CH_2OO + CH_3COCH_3$ at the same temperature and pressure. As a result we believe the change in the absorption intensity of the probe, $A_{375\mathrm{nm}}(t)$, in our system is representative of the concentration of CH_2OO as a function of time:

$$A_{375\ \mathrm{nm}}(t) \propto [CH_2OO](t)$$

From our previous study, the absorption cross section of CH_2OO at 375 nm, $\sigma_{CH_2OO}(375\ \mathrm{nm})$, is (6.2 ± 2.2) × 10^{-18} cm^2 $molecule^{-1}$.[19] For further discussion of the absorption spectrum of CH_2OO see Ting et al.[20]

Once generated, CH_2OO radicals undergo reactions with the co-reactants CH_3COCH_3/CH_3CHO (k_2, k_3) and are also removed from the center of the reactor by other processes. Possible removal processes of CH_2OO in our system include:

$$CH_2OO + CH_3COCH_3 \xrightarrow{k_2} \text{Product}$$

$$CH_2OO + CH_3CHO \xrightarrow{k_3} \text{Product}$$

$$CH_2OO + CH_2OO \xrightarrow{k_{self}} \text{Products}$$

$$CH_2OO + I \xrightarrow{k_{CH2OO+I}} \text{Products}$$

$$CH_2OO \xrightarrow{k_4} \text{Products}$$

Reactions are carried out under pseudo first order conditions, where the co-reactant, CH_3COCH_3 or CH_3CHO, is put in great excess over the initial concentration of CH_2OO and I, so the first-order processes dominate. Most of the radicals react with the species which is in excess. This simplifies the analysis of the transient concentration data greatly, as the kinetics can be accurately fitted by a single exponential function of the form $a \exp(-k't) + c$, black dashed line in Fig. 1.

In most of our absorption experiments, the maximum [CH_2OO] is small enough, 4.9×10^{11} molecule cm^{-3}, that the second-order reaction is negligible. The rate constant for the self-reaction of CH_2OO was reported recently by Buras et al., [19] Ting et al.,[21] and Pun et al.[22] Employing an average value of $k_{self} = 7 \times 10^{-11}$ cm^3 $molecule^{-1}$ s^{-1} and the upper bound rate coefficient for CH_2OO + I of 1×10^{-11} cm^3 $molecule^{-1}$ s^{-1},[19] the computed removal by second order processes is always less than 35 s^{-1}, at least an order of magnitude slower than the first-order processes. Therefore once the CH_2OO formation process is complete, the measured exponential decay of the signal due to CH_2OO absorption in our system can be described by a simple equation:

$$A_{375}(t) = a \exp(-k'_{\text{total}} t) + c \qquad (1)$$

$$k'_{\text{total}} = k_{\text{co-reactant}}[\text{co} - \text{reactant}] + k'_4 \qquad (2)$$

where k'_4 is a catch-all rate that captures effects such as diffusion out of the probe beam, reaction with contaminants and unimolecular decomposition of CH_2OO, a is a scaling factor and c is a vertical offset.

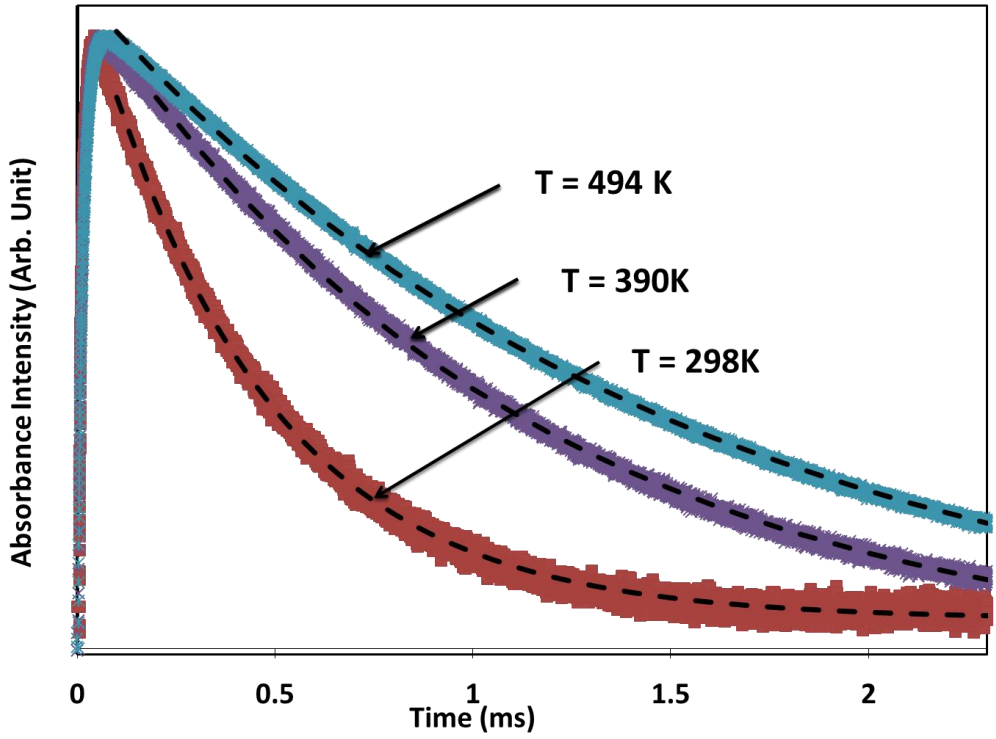

Figure 1. Time resolved CH_2OO absorption signal at 3 temperatures for *P* = 25 Torr, $[O_2]$ = 6 × 10^{16} molecules cm^{-3}, $[CH_2I_2]$ = 1.4 × 10^{14} molecules cm^{-3} and $[CH_3CHO]$ = 1.0 × 10^{15} molecules cm^{-3}. The dashed lines are single exponential fits. The reaction is fastest at low *T*.

A single exponential function was able to fit the absorption traces well at all temperatures less than 500 K. The resultant pseudo-first order plots at 298 K, as shown in Fig. 2, squares, have a relatively small intercept, k'_4, compared to the total removal rate in the presence of the maximum concentration of the co-reactant. This observation demonstrates that reactions with CH_3COCH_3/CH_3CHO are the dominant consumption routes for CH_2OO radicals at room temperature. However, as the temperature increases, triangles and circles in Fig. 2, the title reactions become slower, and the secondary chemistry becomes competitive. Attempts to measure the rate of the title reactions at temperatures above 500 K were made, but, as we have previously shown,[8] even at low photolysis energy (50 mJ/pulse) and low CH_2I_2 concentration, the decay of the CH2OO absorption was fast (~2000 s^{-1}) and not very sensitive to the concentration of the co-reactant, so we could not accurately determine k_2 or k_3. We hypothesize that this is due to the onset of fast unimolecular decomposition at T>500 K.

Control experiments were carried out at different experimental conditions of $[CH_2I_2]$ and photolysis energy. The results are consistent with the base condition ($[CH_2I_2]$ = 1.4 × 10^{14} molecules cm^{-3} and 50 mJ/pulse), implying that the effect of laser energy and precursor

concentration on the measured rate coefficients is negligible. The conditions and results of the control experiment are shown in the Supporting Information.

3.2 *T*-dependence of $CH_2OO + CH_3COCH_3$ and $CH_2OO + CH_3CHO$

A series of 375 nm absorption decay profiles were collected at P = 25 Torr under identical O_2 and CH_2I_2 concentrations at different temperatures between 298 K and 500 K. The decay constants, k'_{total}, extracted from each absorption signal were then plotted against the co-reactant concentration at a given temperature. Sample kinetic plots for $CH_2OO+CH_3COCH_3$ and CH_2OO+CH_3CHO at T = 298 K, 390 K and 494 K are shown in Fig. 2.

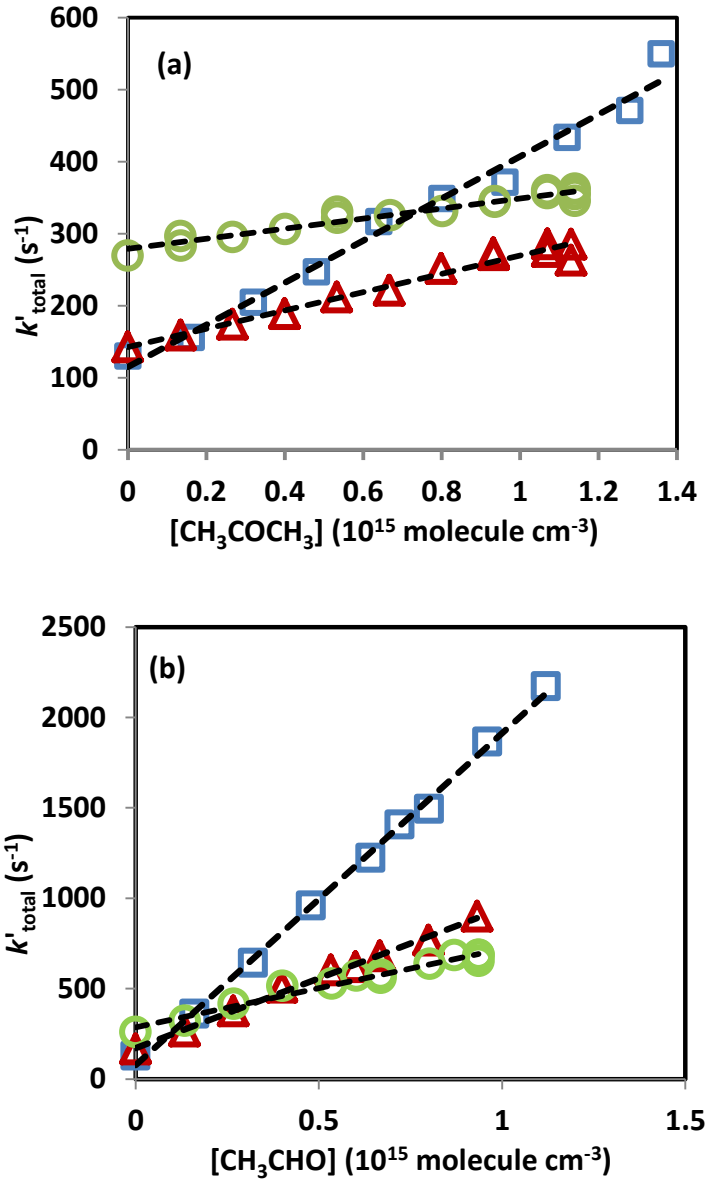

Figure 2. Pseudo-first-order rate coefficient of CH_2OO decay as a function of (a) [CH_3COCH_3] and (b) [CH_3CHO] at P=25 torr and T = 298 K (squares), 390 K (triangles) and 494 K (circles). For discussion of uncertainties, see the text.

Bimolecular rate coefficients for the title reactions (k_2 and k_3) at any given temperature were obtained from the slopes of the k'_{total} vs. [CH_3COCH_3] and [CH_3CHO] plots respectively, Table 1. The decrease in the rate coefficients with temperature reflects the slower removal of CH_2OO by the co-reactant.

Table 1. Bimolecular rate coefficients[a] for the reaction of CH_2OO + CH_3COCH_3, k_2, and CH_2OO + CH_3CHO, k_3, as a function of temperature at P = 25 Torr.

Temperature (K)	k_2 (cm^3 $molecule^{-1}$ s^{-1})	k_3 (cm^3 $molecule^{-1}$ s^{-1})
298	$(3.0 \pm 0.6) \times 10^{-13}$	$(1.2\pm 0.2) \times 10^{-12}$
340	$(1.9 \pm 0.3) \times 10^{-13}$	$(8.0 \pm 1.1) \times 10^{-13}$
390	$(1.3 \pm 0.3) \times 10^{-13}$	$(4.9 \pm 0.8) \times 10^{-13}$
444	$(7.9 \pm 1.9) \times 10^{-14}$	$(3.6 \pm 0.5) \times 10^{-13}$
494	$(7 \pm 2) \times 10^{-14}$	$(2.7 \pm 0.6) \times 10^{-13}$

[a]reported uncertainty includes statistical and systematic errors.

The errors resulting from fitting a single exponential to the measured decay profile are very small ($< 0.1\%$); therefore, error bars are not given for individual k' values, Fig. 2. The main uncertainty in our experiments is due to the imperfect control of the concentrations. We expect maximum systematic errors of ~10% in the reported concentrations due to the uncertainties in the flow controller calibration. As a result, we assumed errors of ±10% for every concentration of the co-reactant to calculate the upper and lower limits of the corresponding rate constants. The reported uncertainties in Tables 1 and 2, and Figs. 3 and 4, include statistical fitting errors as well as our estimates of the maximum systematic error over the T and P range of interest.

Our measured rate coefficients are largely consistent with prior room temperature measurements. At 298 K and 25 torr, our measurement for CH_2OO + CH_3CHO $(1.2 \pm 0.2) \times 10^{-12}$ cm^3 $molecule^{-1}$ s^{-1} is consistent within the uncertainties with the indirect

measurement by Berndt *et al.* (1.7 ± 0.5) × 10^{-12} cm^3 $molecule^{-1}$ s^{-1} and in slight disagreement with Stone *et al.*'s indirect measurement of (1.48 ± 0.04) × 10^{-12} cm^3 $molecule^{-1}$ s^{-1}.[10,12] The kinetics of CH_2OO +CH_3CHO were found to be ~4 times faster than CH_2OO +CH_3COCH_3 across all the temperature range studied here. At 4 torr, our rate coefficients for both reactions are consistent with the room temperature values reported by Taatjes et al.[9]

The temperature dependence of both reactions follows simple Arrhenius kinetics with distinct negative temperature dependence:

$k_2(T) = (7 \pm 2.5) \times 10^{-15}$ cm^3 $molecule^{-1}$ s^{-1} exp[+(9251 ± 2918) J mol^{-1}/RT] (3)

$k_3(T) = (3 \pm 0.8) \times 10^{-14}$ cm^3 $molecule^{-1}$ s^{-1} exp[+(9076 ± 2652) J mol^{-1}/RT] (4)

The variations in k_2 and k_3 with temperature are shown in Fig. 3. Also shown are recently reported rate coefficients for CH_2OO + alkenes measured by Buras *et al.*[8] Such negative temperature dependencies are common for reactions that have a long-range attraction between the reactants and low or submerged reaction barriers.[23] When comparing the reactivity of CH_3CHO and CH_3COCH_3 with our previous data for alkenes (Fig. 3), the differences are obvious. At room temperature, rate coefficients for CH_2OO + carbonyl compounds were found to be two orders of magnitude higher than with alkenes. Considering that reactions of CH_2OO with double bonds[24,25] are expected to proceed mainly *via* 1,3 dipolar cycloaddition,[2] then the increase in the rate coefficients in going from alkenes to carbonyl compounds is likely due to the differences in the nature of the corresponding double bonds. The C=O bond is expected to be more reactive towards CH_2OO on account of its higher dipolar character compared to the C=C bonds in alkenes. The reported pre-exponential factor

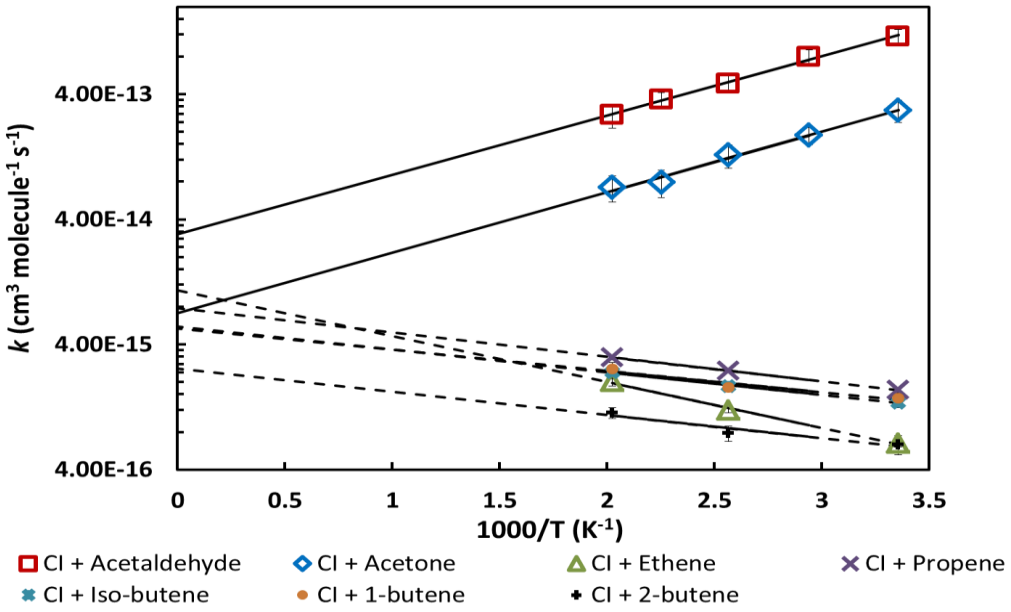

Figure 3. Arrhenius plot of the experimentally determined rate constants for the CH_2OO + CH_3COCH_3, k_2, and CH_2OO + CH_3CHO, k_3, together with the best fit to $k = Aexp(-E/RT)$, solid line, and statistical and systematic errors. Also included are data for CH_2OO + alkenes.[8]

for the reaction of CH_2OO with alkenes[8] is similar to that reported here for the reaction with carbonyl compounds, CH_3COCH_3 and CH_3CHO, implying that the differences in their reactivity towards CH_2OO is due primarily to the depth of the submerged transition state. Further explanation is given in the theory section below.

3.3 *P*-dependence of CH_2OO + CH_3COCH_3 and CH_2OO + CH_3CHO

Experiments were done at P = 4 Torr, 25 Torr and 50 Torr. The corresponding rate coefficients are presented in Fig. 4 and Table 2. Within the uncertainty of our

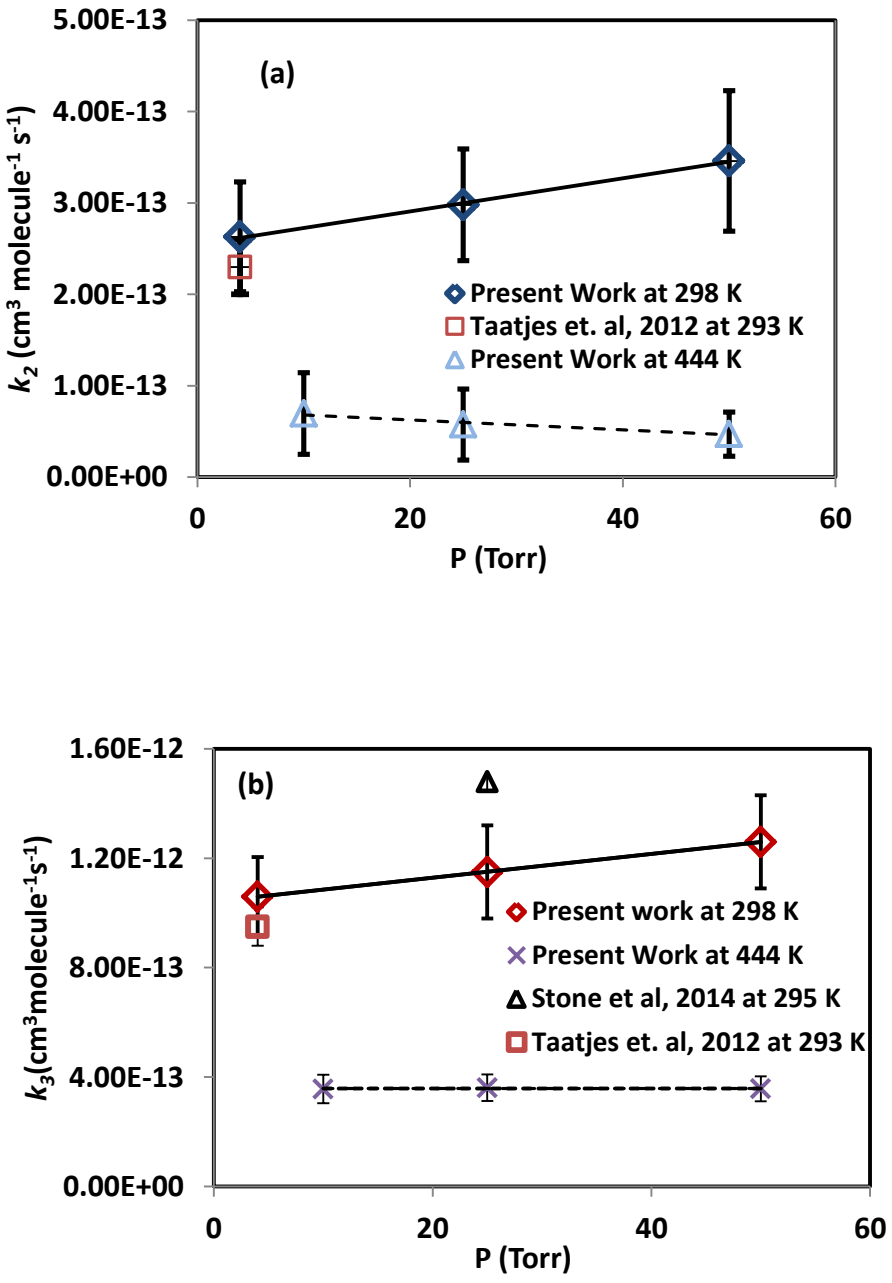

Figure 4. Plot of the pressure-dependence of the rate coefficients for the reactions (a) CH_2OO +CH_3COCH_3, k_2, and (b) CH_2OO + CH_3CHO, k_3. Both statistical (fitting) and systematic errors have been incorporated in the error bars.

measurements, a weak pressure dependence was observed for both reactions at 298 K. Any pressure dependence in the rate coefficients is even harder to discern at 444 K. The difference between the rate coefficients across the measured pressure range of interest is comparable to the uncertainty associated with the individual measurements.

Table 2. Bimolecular rate coefficients[a] for the reaction of CH_2OO + CH_3COCH_3, k_2, and CH_2OO + CH_3CHO, k_3, as a function of pressure at 298 K and 444 K.

Pressure (Torr)	k_2 (cm^3 $molecule^{-1}$ s^{-1})	k_3 (cm^3 $molecule^{-1}$ s^{-1})
a) T = 298 K		
4	$(2.6 \pm 0.6) \times 10^{-13}$	$(1.1 \pm 0.1) \times 10^{-12}$
25	$(3.0 \pm 0.6) \times 10^{-13}$	$(1.2 \pm 0.2) \times 10^{-12}$
50	$(3.5 \pm 0.8) \times 10^{-13}$	$(1.3 \pm 0.2) \times 10^{-12}$
b) T = 444 K		
10	$(8.5 \pm 2.2) \times 10^{-14}$	$(3.6 \pm 0.5) \times 10^{-13}$
25	$(7.9 \pm 1.9) \times 10^{-14}$	$(3.6 \pm 0.5) \times 10^{-13}$
50	$(7.4 \pm 1.2) \times 10^{-14}$	$(3.6 \pm 0.5) \times 10^{-13}$

[a]reported uncertainty includes statistical and systematic errors.

4. TOF-MS results

Because we were not able to detect any products in the mass spectra for the CH_2OO + CH_3CHO system at 25 Torr using 10.5 eV photoionization, the results in this section focus exclusively on CH_2OO + CH_3COCH_3. The time resolved mass spectra for CH_2OO + CH_3COCH_3 was recorded at three different pressures 10, 25 and 50 Torr. In all cases the CH_2OO reactant was observed at m/z = 46 amu. Fig. 5 shows a section of our measured mass spectra for CH_2OO + CH_3COCH_3 as a function of reaction time. Two ions from products were observed, at m/z = 104 amu and 89 amu. The m/z = 104 amu channel is attributed[9] to the parent ion of the secondary ozonide (SOZ), an expected major product. The m/z=89 amu channel was assigned as a daughter ion of another mass 104 species that fragments upon photo-ionization; Taatjes et al. proposed this easily fragmented, mass 104 species is methoxymethyl acetate.[9]

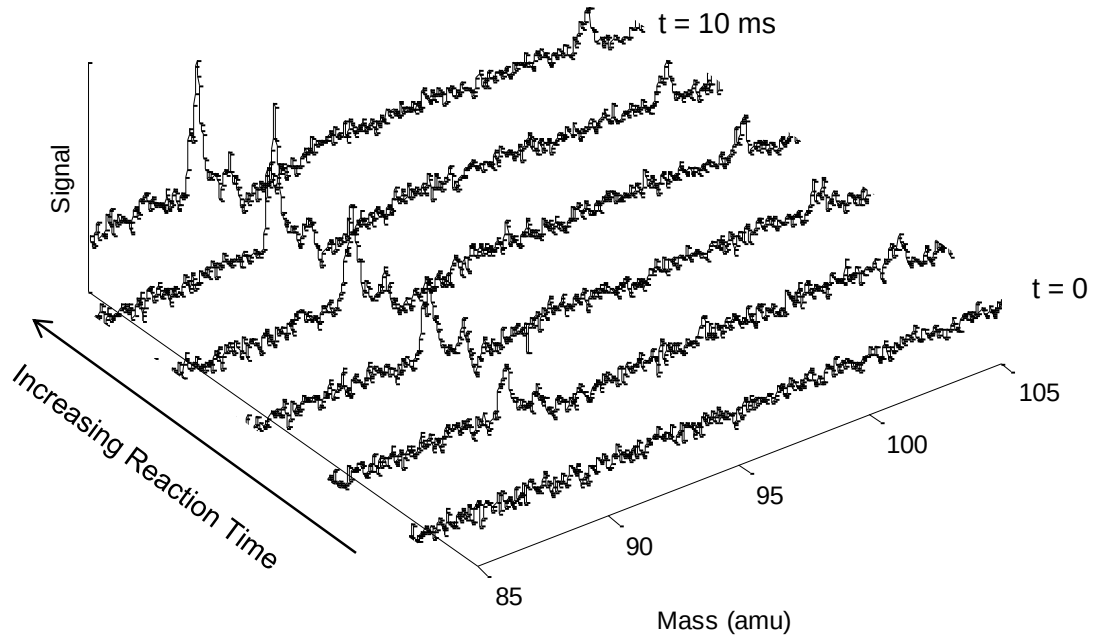

Figure 5. Section of mass spectrum at 298 K, 10 Torr, $[\mathbf{O_2}] = \mathbf{6 \times 10^{16} cm^{-3}}$, $[\mathbf{CH_2I_2}] = \mathbf{2.44 \times 10^{14} cm^{-3}}$ and $[\mathbf{CH_3COCH_3}] = \mathbf{1.24 \times 10^{15} cm^{-3}}$ showing time dependence of two product peaks of CH_2OO + CH_3COCH_3: $\frac{m}{z} = \mathbf{89}$ and **104** amu. The spectrum at $\boldsymbol{t = -0.2}$ **ms** has been subtracted so that only species formed following the photolysis flash at t=0 are evident.

To achieve sufficient signal-to-noise ratio, a higher $[CH_2OO]$ was used in the mass spectrometry experiments than in the absorbance experiments reported above, increasing the contribution from the self-reaction of CH_2OO (k_{self}). Therefore, the self-reaction of CH_2OO is included in the kinetic model for CH_2OO + CH_3COCH_3, as shown in Scheme 1. Once formed in the presence of acetone, CH_3COCH_3, we assume that CH_2OO can react with CH_3COCH_3 (k_2), react with itself (k_{self}), or unimolecularly decompose/diffuse out of the sampling volume (k_4). The product branching fractions to SOZ, methoxymethyl acetate, and formic acid are represented by β_{104}, β_{89}, and β_{46}. Formic acid is expected to be a major product[15], but we cannot observe this channel because the ionization energy (IE) of formic acid is larger than 10.5 eV.[26] The kinetic model is shown in Scheme 1.

$$CH_2OO + CH_3COCH_3 \xrightarrow{k_2} \text{Products} \xrightarrow{\beta_{89}} \text{Product which forms } \frac{m}{z} = 89$$

$$\xrightarrow{\beta_{104}} \frac{m}{z} = 104 \text{ Product (SOZ)}$$

$$\xrightarrow{\beta_{46}} HCOOH + CH_3COCH_3$$

$$CH_2OO \xrightarrow{k_4} \text{Products}$$

$$2\,CH_2OO \xrightarrow{k_{self}} \text{Products}$$

$$[CH_2OO](t = 0) = [CH_2OO]_0$$

Scheme 1. General kinetic model for CH_2OO + CH_3COCH_3, CH_2OO + I reaction is not included in the model for its insignificant effect.

This kinetic model is consistent with the measured time-dependence, Fig. 6, though at long times the stable product signals decline, presumably due to diffusion out of the volume illuminated by the photolysis laser.

We couldn't determine absolute product branching fractions of the CH_2OO + CH_3COCH_3 reaction, β_i (where $i = 89$ or 104), as the photoionization cross section for the products, σ_{89} and σ_{104}, are not known. However, we can ratio the measured value of $\sigma_i\beta_i$ at one pressure to another pressure. Assuming σ_i is pressure-independent, then the relative pressure dependent yield of product i is given by the following mathematical expression:

$$\frac{(\beta_i)_{P1}}{(\beta_i)_{P2}} = \frac{\left(\frac{S_i(t\to\infty)}{\bar{S}_{calmix,j}} \frac{[calmix,j]}{[\text{Products}_{(CI+\text{Acetone})}](t\to\infty)}\right)_{P1}}{\left(\frac{S_i(t\to\infty)}{\bar{S}_{calmix,j}} \frac{[calmix,j]}{[\text{Products}_{(CI+\text{Acetone})}](t\to\infty)}\right)_{P2}} \qquad (5)$$

Where S_i is the integrated MS peak area for the species i, $\bar{S}_{calmix,j}$ is the average value of the integrated peak area of MS signals for one of the calibration mixture species used as internal standards, j,$\sigma_i(E)$ is the photoionization cross-section of species i at energy E, $[calmix,j]$ is the concentration of calibration species j, and $[Products]_{CI+Acetone}$ $(t \to \infty)$ is the steady state concentration of all CH_2OO + Acetone products. An analytical expression for $[Products]_{CI+Acetone}$ $(t \to \infty)$ obtained by solving the kinetic model represented by Scheme 1 is given in the Supporting Information along with details of how it is quantified. A full derivation of Eq. 5 is also provided in the Supporting Information.

$S_i(t \to \infty)$ and $\bar{S}_{calmix,j}$ are determined from the PI TOF-MS data as shown in Fig. 6 and Fig. S4. If the product species concentration was constant after being formed, then the value of $S_i(t \to \infty)$ would simply be the TOF-MS signal at long times. However, the products do undergo subsequent reactions and they also diffuse out of the sampling volume as manifested by a slow, but noticeable decay in signal. Therefore, $S_i(t \to \infty)$ is obtained by first fitting $S_{46}(t)$, $S_{89}(t)$ and $S_{104}(t)$to the kinetic model shown in Scheme 1 with the addition of a first-order loss term for the 89 and 104 amu products (solid lines in Fig. 6). The fit model is then simulated without the first order loss-terms for 89 and 104 amu (dashed lines in Fig. 6) and $S_i(t \to \infty)$ is taken as the values of these simulations at long time. $S_{calmix,j}(t)$ was recorded simultaneously as $S_i(t)$ and averaged over all of the time points to obtain $\bar{S}_{calmix,j}(t)$ as indicated by the line in Fig. S4. Control experiments were conducted at the same conditions as the experiment in Fig. 6, but without CH_3COCH_3, O_2 or the calibration mixture to support the identification of the $\frac{m}{z} = 89$ amu and $\frac{m}{z} = 104$ amu species as products of CH_2OO + CH_3COCH_3 and not as products of something else. Details of the control experiments are in the Supporting Information.

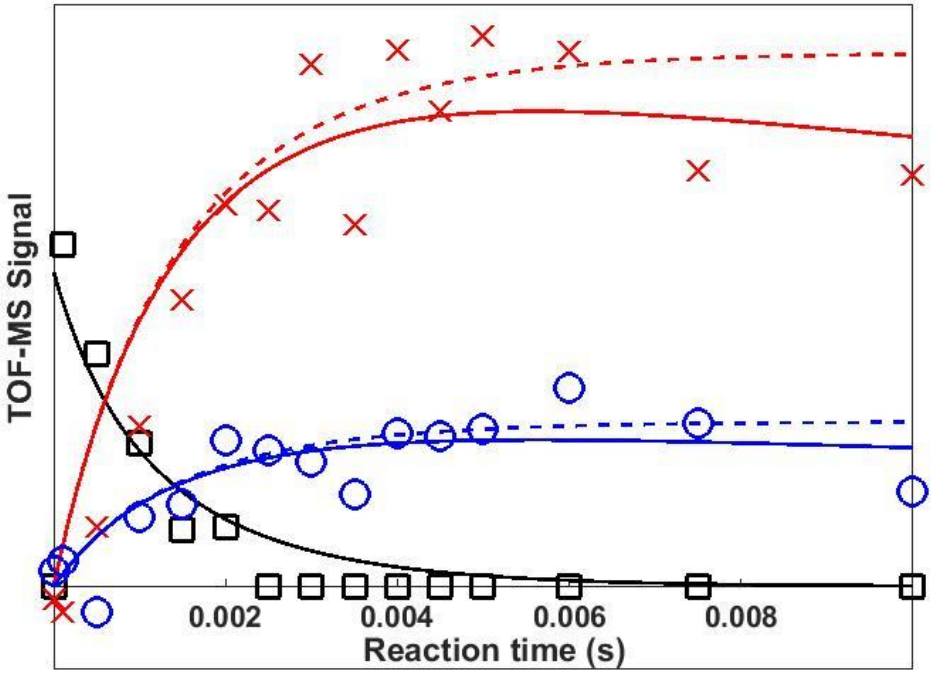

Figure 6. Measured TOF-MS signals at 298 K, 10 Torr, $[\mathbf{O_2}] = \mathbf{5.95 \times 10^{16} cm^{-3}}$ and $[\mathbf{CH_3COCH_3}] = \mathbf{1.24 \times 10^{15} cm^{-3}}$ for $\frac{\boldsymbol{m}}{\boldsymbol{z}} = \mathbf{46\ amu}$ (black squares), $\frac{\boldsymbol{m}}{\boldsymbol{z}} = \mathbf{89\ amu}$ (red crosses) and $\frac{\boldsymbol{m}}{\boldsymbol{z}} = \mathbf{104\ amu}$ (blue circles) recorded simultaneously as the benzene internal standard signal shown in Fig. S4. The lines are fits to the kinetic model described by Scheme

1 with (solid) and without (dashed) the addition of first-order loss terms for the 89 and 104 amu products. $\boldsymbol{S_i(t \to \infty)}$ is taken as the maximum value of the dashed lines. Note that the signal at $\boldsymbol{t = -0.20\ ms}$ was subtracted from all subsequent time points so that the signal is roughly zero at $\boldsymbol{t = 0}$.

Figure 7 shows the measured values of $\frac{(\beta_i)_{P1}}{(\beta_i)_{P2}}$ for $\frac{m}{z} = 89$ amu. The error bars are from propagation of uncertainty. The yield of the species leading to the $\frac{m}{z} = 89$ amu signal increases by about a factor of 2 as the pressure is increased from 10 torr to 25 torr and then stabilizes. For $\frac{m}{z} = 104$ amu, however, the TOF-MS signal was too low to discern a trend with respect to pressure (see Fig. S5). The relative pressure dependent yield of SOZ in a He bath gas predicted by Jalan et al.[15] is also shown in Fig. 7 for comparison. The measured P-dependence of the 89 amu signal is quite different from the P-dependence predicted for SOZ, supporting the hypothesis that the 89 amu signal is coming from a different species, not SOZ.

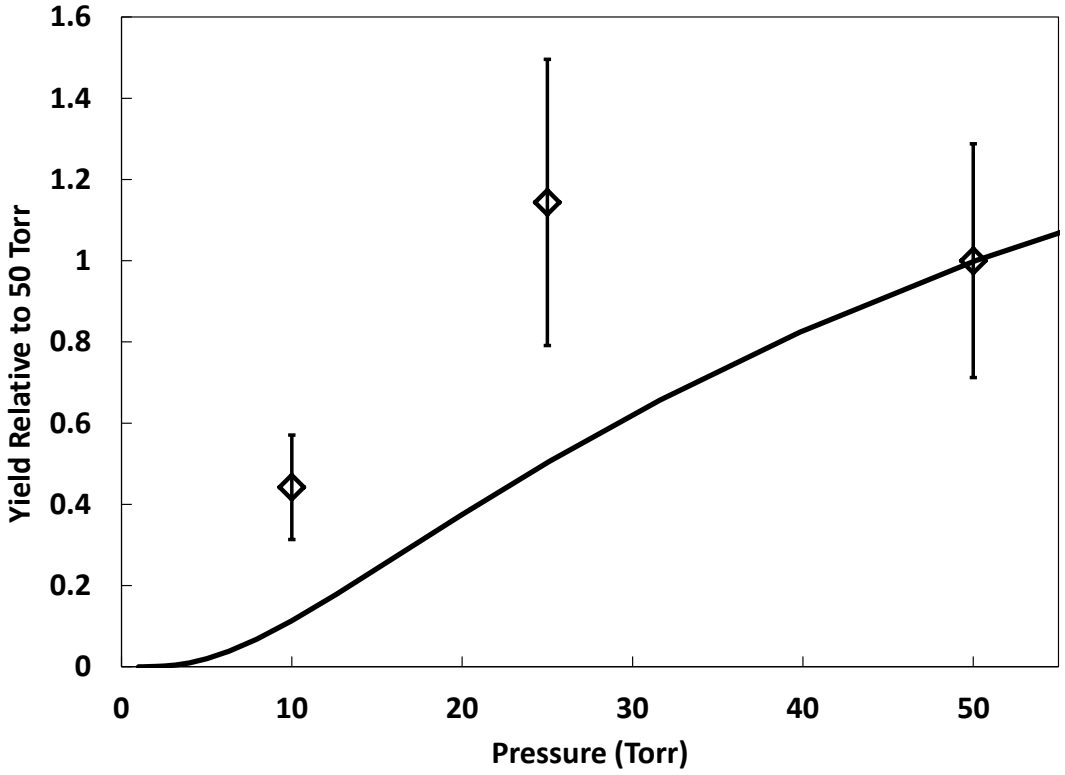

Figure 7. Relative yield of $\frac{m}{z} = 89$ amu product from CH_2OO + CH_3COCH_3 normalized to the 50 Torr measurement $\left(\frac{(\beta_{89})_{P=X\ Torr}}{(\beta_{89})_{P=50\ Torr}}\right)$ at 298 K (markers) compared to predicted relative yield of SOZ at the same conditions from Jalan et al.[15] (line).

The relative ratio of $\frac{\beta_{89}}{\beta_{104}}$ can be determined by the following equation.

$$\frac{\left(\frac{\beta_{89}}{\beta_{104}}\right)_{P1}}{\left(\frac{\beta_{89}}{\beta_{104}}\right)_{P2}} = \frac{\left(\frac{S_{89}(t\to\infty)}{S_{104}(t\to\infty)}\right)_{P1}}{\left(\frac{S_{89}(t\to\infty)}{S_{104}(t\to\infty)}\right)_{P2}} \qquad (6)$$

The results are shown in Fig. 8 below. Because of the weakness of the $\frac{m}{z} = 104$ amu signal the error bars are large and we cannot determine conclusively if the ratio is P-dependent.

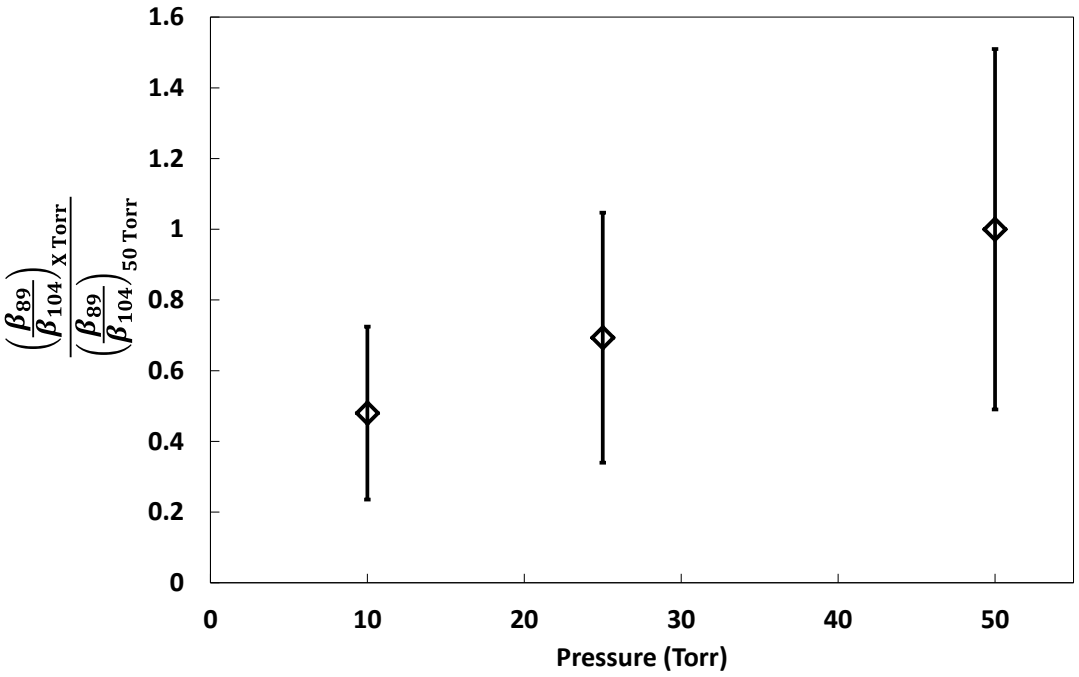

Figure 8. Ratio of $\frac{m}{z} = 89$ to $\frac{m}{z} = 104$ amu product yield from CH_2OO + CH_3COCH_3 normalized to the 50 Torr measurement ($\frac{\left(\frac{\beta_{89}}{\beta_{104}}\right)_{\text{X Torr}}}{\left(\frac{\beta_{89}}{\beta_{104}}\right)_{\text{50 Torr}}}$).

The results of our MS experiments agree qualitatively with the previous results of Taatjes *et al.*,[9] in that the only products observed from the reaction CH_2OO + CH_3COCH_3 are at m/z = 104 and m/z = 89 (they also did not go to high enough ionization energies to see formic acid) and the MS signal for the latter is about 5 times more intense than that of the former. All of our results are discussed in the context of Jalan *et al.*'s predictions of the overall rate coefficient and the product branching in the following section. [15]

5. Theoretical analysis of temperature dependence and product branching

As shown by Jalan *et al*.,[15] the entrance channel for the title reactions is characterized by two transition states: a loose *outer* transition state (TS_{outer}) leading to the formation of the Van der Waals (VdW) complex and an *inner* 1,3-cycloaddition transition state (TS_{inner}) leading to the secondary ozonide (SOZ). Either of these transition states can be rate-limiting depending on the temperature and pressure of interest. Figure 9 depicts the entrance channel for both reactions and the simple phenomenological mechanism employed to model this process.

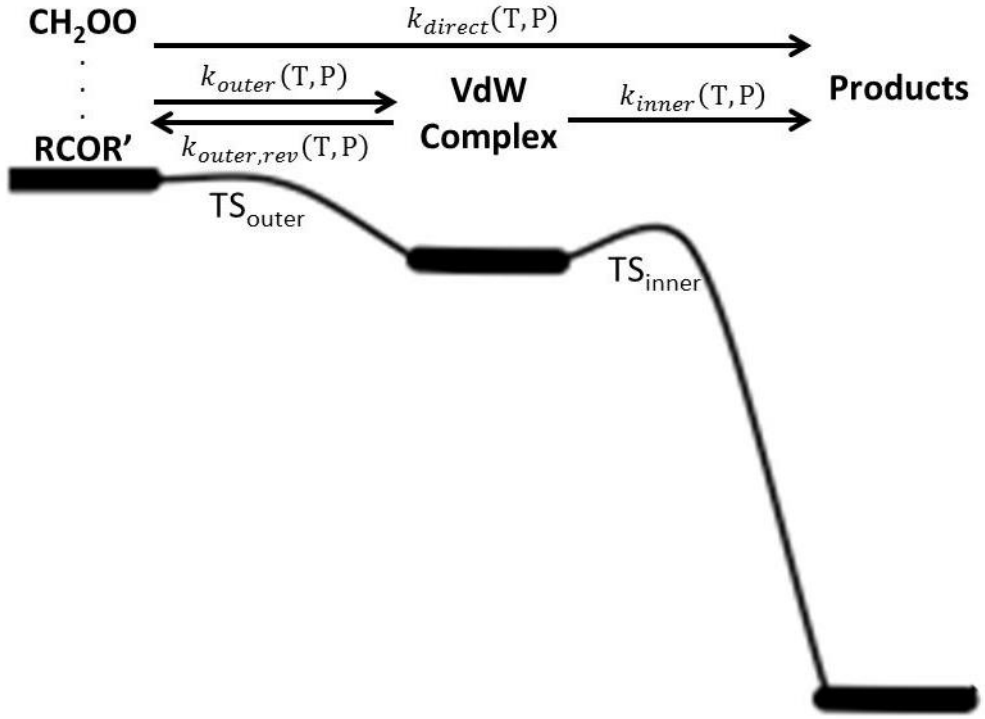

Figure 9. Schematic of entrance channel PES for CH_2OO + CH_3CHO/CH_3COCH_3. Relative energies for VdW and TS_{inner} are -7.3 kcal/mol and -5.3 kcal/mol for the CH_2OO + CH_3CHO system respectively and are -7.6 kcal/mol and -4.9 kcal/mol for the CH_2OO + CH_3COCH_3 system (including zero point corrections).[15]

As shown, the reactants may either skip directly to the SOZ and other products *via* a chemically activated process with T,P-dependent rate coefficient k_{direct}, or they may be stabilized in the VdW complex well with a rate coefficient k_{outer}. However, owing to its shallow well, even the stabilized VdW complex has a very short lifetime, and it will either redissociate to the reactants, $k_{outer,rev}$, or cross TS_{inner}, k_{inner}. Applying the pseudo-steady-state approximation (PSSA) to the VdW complex and assuming pseudo-first-order conditions with respect to the carbonyl, one arrives at the following

equation for the experimentally observable second-order rate coefficient for the decay of CH_2OO, $k_{observable}$.

$$k_{observable}(\mathrm{T,P}) = k_{direct}(\mathrm{T,P}) + k_{outer}(\mathrm{T,P})\left(\frac{k_{inner}(\mathrm{T,P})}{k_{outer,rev}(\mathrm{T,P}) + k_{inner}(\mathrm{T,P})}\right) \quad (7)$$

Cantherm, a computer code developed as part of the RMG-Py software package,[27] was used to obtain values for all of the T,P-dependent k's in Eq. 7 by solving the 1-D master equation using the Reservoir State approximation (the same results are obtained in the low- and high-pressure limits using the Modified Strong Collision approximation). All inputs to Cantherm (electronic energies, vibrational frequencies, rotational constants and hindered rotor scans for all stationary points, as well as the collisional energy transfer model) were supplied by the calculations of Jalan *et al.*[15] The only remaining input left to be specified is k_{outer} in the high-pressure limit, $k_{outer}^{P=\infty}(\mathrm{T})$. This is because TS_{outer}, as a loose barrierless transition state, would require a variable reaction coordinate (VRC-TST) treatment to be located accurately. Instead, by supplying an estimate of $k_{outer}^{P=\infty}(\mathrm{T})$, microcanonical rate coefficients, $k_{outer}(\mathrm{E})$, can be obtained from the inverse Laplace transform of $k_{outer}^{P=\infty}(\mathrm{T})$.[28]

A reasonably accurate estimate of $k_{outer}^{P=\infty}(\mathrm{T})$ can be obtained using analytical expressions from Georgievski and Klippenstein[29] for typical long-range interactions between reacting fragments. These analytical expressions rely on estimates of the dipole moment, quadrupole moment and polarizability of the reacting fragments in addition to the masses. For the systems of interest here, these properties were estimated using the B3LYP density functional with the MG3S basis set used by Jalan *et al.* for the CH_2OO + CH_3CHO and CH_2OO + CH_3COCH_3 potential energy surfaces.[15] Ionization energies (required for estimating the contribution from dispersion interactions) for CH_3CHO and CH_3COCH_3 were obtained from the NIST Chemistry Webbook while the value for CH_2OO was obtained from the work of Lee et al.[30] The contributions from each of the long-range interactions for CH_2OO + CH_3CHO and CH_2OO + CH_3COCH_3 are shown in Table 3.

Table 3: Contributions from various long-range interactions to the overall capture rate $\boldsymbol{k_{outer}^{P=\infty}(T)}$ for CH_2OO + CH_3CHO and CH_2OO + CH_3COCH_3. All rate expressions in units of ($\mathbf{10^{-10}}$ cm^3 molecule^{-1} sec^{-1}) and temperatures in K.

Interaction	CH_2OO + CH_3CHO ($\mathbf{10^{-10}}$ cm^3 molecule^{-1} sec^{-1})	CH_2OO + CH_3COCH_3 ($\mathbf{10^{-10}}$ cm^3 molecule^{-1} sec^{-1})

Dipole-dipole	$21.39\ T^{-\frac{1}{6}}$	$20.17\ T^{-\frac{1}{6}}$
Dipole-induced dipole	7.17	6.80
Induced dipole – induced dipole	$1.42\ T^{\frac{1}{6}}$	$1.45\ T^{\frac{1}{6}}$
Dispersion	$1.88\ T^{\frac{1}{6}}$	$1.89\ T^{\frac{1}{6}}$

For the purpose of our master equation calculations, only the most significant long-range interaction (the dipole-dipole interaction) was used for $k_{outer}^{P=\infty}(T)$ because the various contributions cannot simply be summed together. Furthermore, as will be shown later, our results are largely insensitive to the absolute value of $k_{outer}^{P=\infty}(T)$ in our T and P range.

Figure 10 compares our calculation of $k_{observable}$ for both reactions at 298 and 444 K as a function of pressure with the experimental measurements. Also shown is the predicted branching to the major products, computed using a modified version of Eq. 7 where k_{direct} and k_{inner} are for specific products rather than the sum of all products. Clearly there are low and high-P limits to $k_{observable}$ in all cases, although the difference becomes less pronounced at higher temperatures. The difference between $k_{observable}^{P=0}$ and $k_{observable}^{P=\infty}$ is due to the states of TS_{inner} below the energy of the separated reactants being inaccessible in the collisionless low-P limit. In the high-P limit, these submerged states are populated and $k_{observable}$ increases correspondingly. At higher temperatures, the inclusion or exclusion of the submerged TS_{inner} states matters less, as more of the higher energy states are populated, and these dominate the rate.

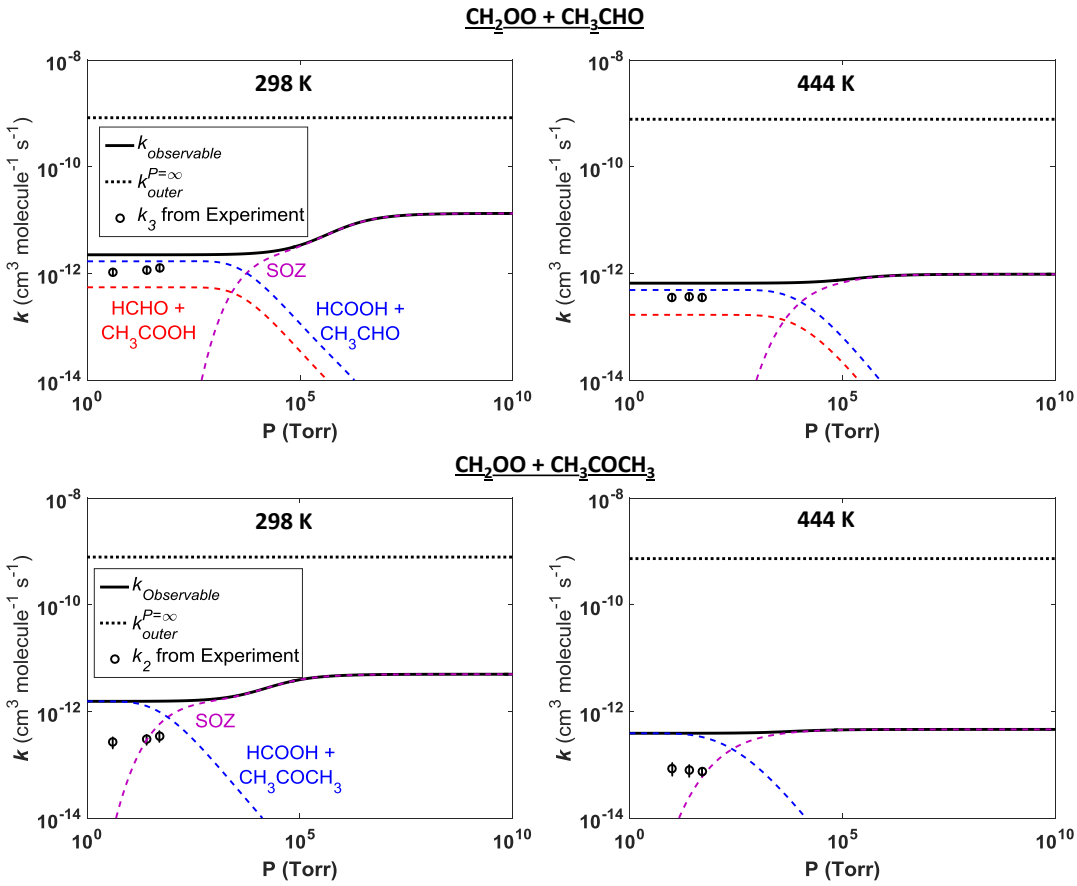

Figure 10. Predicted P-dependence for CH_2OO + CH_3CHO (upper)/CH_3COCH_3 (lower). Black dots represent experimental measurements for overall CH_2OO + CH_3CHO and CH_2OO + CH3COCH$_3$ rate coefficients, k_3 and k_2, respectively.

The bottleneck to $k_{observable}$ in both the low and high-P limits over the temperature range of interest to us (298-500 K) is TS_{inner}. This is demonstrated for $k_{observable}^{P=0}$ by varying $k_{outer}^{P=\infty}(\mathrm{T})$ over two orders of magnitude (Fig. S6). As shown, increasing $k_{outer}^{P=\infty}(\mathrm{T})$ by a factor of ten has a negligible effect on $k_{observable}^{P=0}$, while decreasing it by a factor of ten has a more noticeable, but still small impact on $k_{observable}^{P=0}$.

In the high-P limit, $k_{direct}(\mathrm{T},\mathrm{P}) = 0$ and Eq. 7 simplifies to the following.

$$k_{observable}^{P=\infty}(\mathrm{T}) = k_{outer}^{P=\infty}(\mathrm{T})\left(\frac{k_{inner}^{P=\infty}(\mathrm{T})}{k_{outer,rev}^{P=\infty}(\mathrm{T}) + k_{inner}^{P=\infty}(\mathrm{T})}\right) \quad (8)$$

If $k_{outer}^{P=\infty}(\mathrm{T})$ was rate-limiting, then $k_{outer,rev}^{P=\infty}(\mathrm{T}) \ll k_{inner}^{P=\infty}(\mathrm{T})$ and Eq. 8 would simplify to $k_{outer}^{P=\infty}(\mathrm{T})$. This is clearly not the case, because, as shown in Fig. 10, in the high-P limit $k_{observable}^{P=\infty}(\mathrm{T})$ is three orders of magnitude smaller than $k_{outer}^{P=\infty}(\mathrm{T})$

(shown by the dotted black line). Furthermore, if $k_{inner}^{P=\infty}(\mathrm{T})$ is indeed rate-limiting in the high-P limit, $k_{outer,rev}^{P=\infty}(\mathrm{T}) \gg k_{inner}^{P=\infty}(\mathrm{T})$ and Eq. 8 simplifies further.

$$k_{observable}^{P=\infty}(\mathrm{T}) = \frac{k_{outer}^{P=\infty}(\mathrm{T})}{k_{outer,rev}^{P=\infty}(\mathrm{T})} k_{inner}^{P=\infty}(\mathrm{T}) \quad (9)$$

Using canonical TST expressions for the three high-P k's above results in a simple expression for $k_{observable}^{P=\infty}(\mathrm{T})$:

$$k_{observable}^{P=\infty}(\mathrm{T}) = \frac{k_B T}{h} \frac{\left(\frac{Q_{TS,outer}}{Q_{reactants}}\right)\left(\frac{Q_{TS,inner}}{Q_{VdW\ complex}}\right)}{\left(\frac{Q_{TS,outer}}{Q_{VdW\ complex}}\right)} \times \exp\left(-\frac{\left[\left(E_0^{TS,outer} - E_0^{reactants}\right) + \left(E_0^{TS,inner} - E_0^{VdW}\right) - \left(E_0^{TS,outer} - E_0^{VdW}\right)\right]}{RT}\right) \quad (10)$$

$$k_{observable}^{P=\infty}(\mathrm{T}) = \frac{k_B T}{h}\left(\frac{Q_{TS,inner}}{Q_{reactants}}\right) \times \exp\left(-\frac{\left[E_0^{TS,inner} - E_0^{reactants}\right]}{RT}\right) \quad (11)$$

where E is the zero-point inclusive energy and Q is the partition function per unit volume for a given species, relative to that species' zero point energy. Equation 11 is the canonical TST equation one would obtain by simply ignoring TS_{outer} and the VdW complex and is therefore denoted k_{TST}. Figure 11 compares $k_{observable}^{P=0}(\mathrm{T})$, $k_{observable}^{P=\infty}(\mathrm{T})$ from Eq. (8), and $k_{TST}(\mathrm{T})$ along with our experimental measurements. $k_{TST}(\mathrm{T})$ is virtually indistinguishable from $k_{observable}^{P=\infty}(\mathrm{T})$, because the inner transition state is rate-limiting.

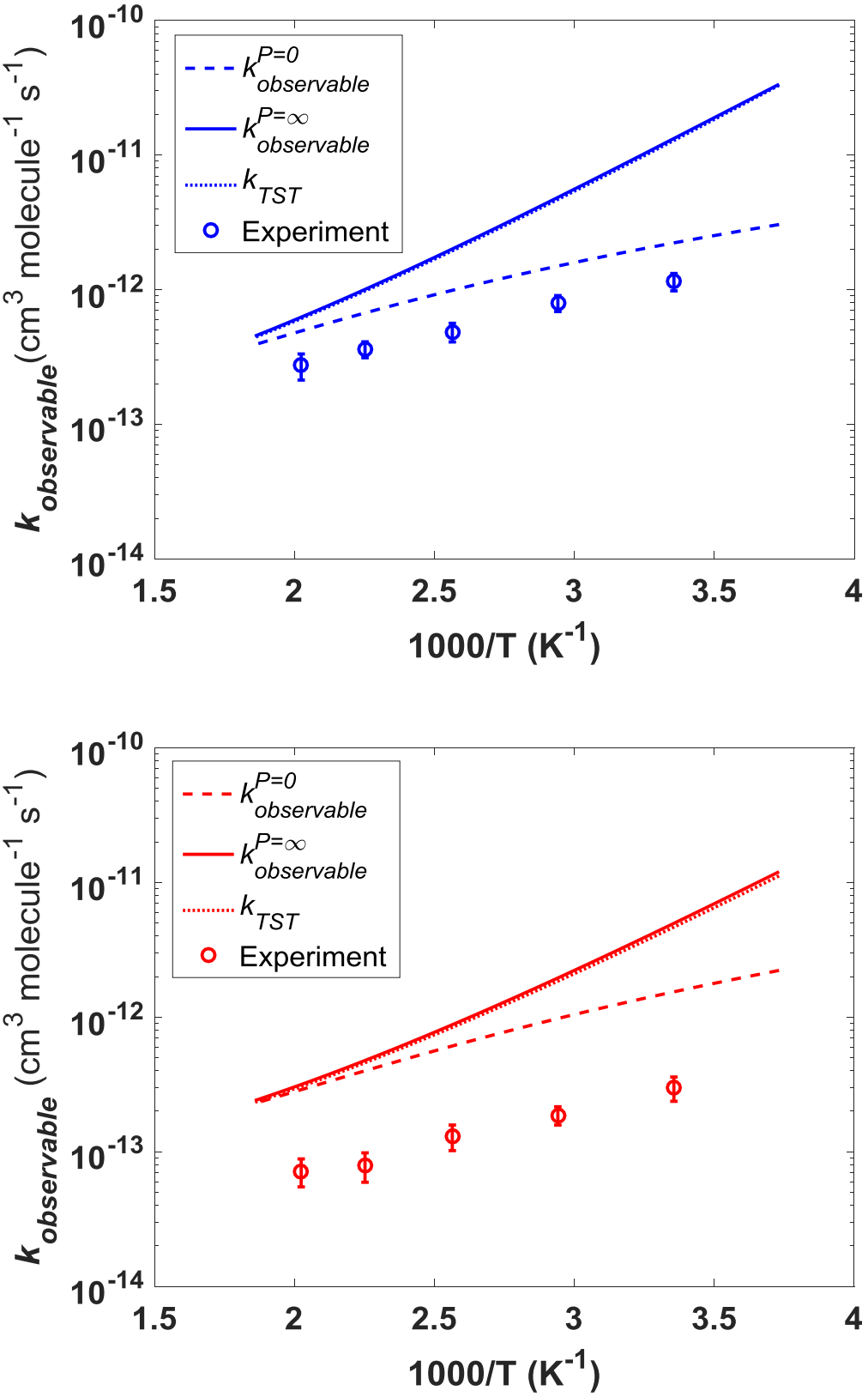

Figure 11. Predicted T-dependence for CH_2OO + CH_3CHO (upper)/CH_3COCH_3 (lower) in the low- and high-pressure limits, $k_{observable}^{P=0}(T)$ and $k_{observable}^{P=\infty}(T)$, respectively. Predictions of simple TST calculations are also shown, $k_{TST}(T)$. Blue

and red dots represent experimental measurements for CH_2OO + CH_3CHO and CH_2OO + CH_3COCH_3, respectively (P = 25 Torr in Helium).

For both CH_2OO + CH_3CHO and CH_2OO + CH_3COCH_3, Fig. 10 suggests that our experimental measurements were conducted in the low-P limit with respect to $k_{observable}$, which is consistent with the lack of P-dependence observed for either k_2 or k_3. In the case of CH_2OO + CH_3CHO, $k_{observable}^{P=0}(T)$ is within a factor of two of experiment, whereas for CH_2OO + CH3COCH$_3$ $k_{observable}^{P=0}(T)$ is higher by about a factor of five. We observed a similar order of magnitude discrepancy between predictions and measurements for the case of CH_2OO + alkenes,[8] which we attribute mostly to uncertainty in the PES. Table 4 compares simple Arrhenius fits between the predictions (P=0) and experiment. It appears from the discrepancy between the model predictions and the experimental data that the theoretically calculated A-factors are mostly at fault, whereas the computed submerged barrier heights give Ea's in remarkable agreement with experiment.

Table 4: Theoretical Arrhenius parameters in the low-pressure limits (in units of A: cm^3/molecule/sec and E_a: kcal/mole) for the CH_2OO + CH_3CHO and CH_2OO + CH_3COCH_3 systems for T in the 300-500 K range. Experimentally determined values shown for comparison.

System		Theory $P = 0$	Experiment (P = 25 Torr in He)
CH_2OO + CH_3CHO	A	6.6×10^{-14}	$(3 \pm 0.8) \times 10^{-14}$
	E_a	-2.1	-2.2 ± 0.6
CH_2OO + CH_3COCH_3	A	2.8×10^{-14}	$(7 \pm 2.5) \times 10^{-15}$
	E_a	-2.4	-2.2 ± 0.7

Product branching in CH_2OO + CH_3CHO and CH_2OO + CH_3COCH_3 has already been discussed in detail by Jalan *et al.*[15] who used detailed RRKM/Master equation calculations to provide evidence for organic acid formation at low-pressures. Similar calculations of the product distribution, shown in Fig. 10, suggest that the acetaldehyde system is in the low-pressure limit for the product distribution under the current experimental conditions (P = 4 to 50 Torr in Helium). In contrast, the acetone system is predicted to exhibit notable pressure dependence in the product branching over the same pressure range, which is qualitatively consistent with the P-dependence of the m/z = 89 isomer yield shown in Fig. 7. However, the CH_2OO + CH_3COCH_3 PES used

does not include a m/z = 104 isomer other than SOZ that is produced in significant quantities. Our TOF-MS results and prior work by Taatjes *et al.*[9] strongly suggests another m/z =104 adduct is formed, probably in higher concentration than the SOZ. Our work (Fig. 7) even suggests that this adduct might be in its high-P limit in 50 Torr He. Further investigation of this PES would be most beneficial to understanding these experimental results.

The high yield of 88% HCHO from CH_2OO+CH_3CHO in 4 Torr N_2 estimated by Stone *et al.*,[10] appears to be in disagreement with our predicted low-pressure product distribution in Fig. 10, where HCHO accounts for only ~25% of the yield. However, this discrepancy can be explained by taking into consideration the uncertainties in both the measurements and predictions, as detailed in the SI. Qualitatively, their measured decrease in HCHO yield with pressure is consistent with our predictions.

Calculations of k_{TST} were also conducted up to 2000 K and compared to identical calculations for CH_2OO + alkenes[8] in order to evaluate the real A factors as $T \rightarrow \infty$. Similar to Fig. 3, Fig. 12 shows that although values of k for CH_2OO + carbonyls are 2-3 orders of magnitude higher than for CH_2OO + alkenes at room T, as T increases the two sets of k values merge to within a factor of two of each other. This demonstrates that the A factor (entropic term) is similar for CH_2OO + C=O and C=C cycloadditions and the large difference in k's at room temperature is almost entirely due to the energetic difference of the reaction barrier. The strong curvature of the carbonyl predictions at high T is due to the emerging dominance of the entropic term. Specifically, the positive temperature dependence of the ratio of inner TS to reactant vibrational partition functions dominates over other contributions at high T (Fig. S7). The larger k for the acetaldehyde reaction as compared to acetone over the entire T range is attributable partly to the 0.4 kcal/mol difference in submerged TS_{inner} barrier heights and partly to the larger A-factor for the former (again see Fig. S7)

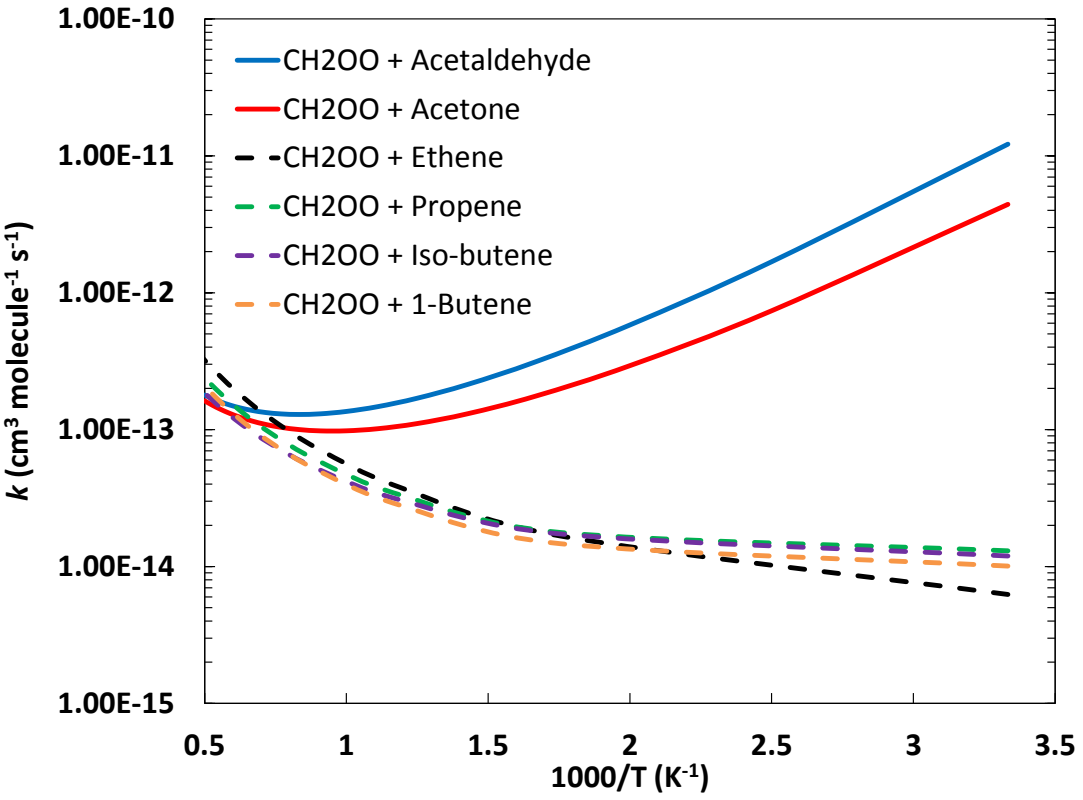

Figure 12. Predicted *T*-dependence for CH_2OO + carbonyls/alkenes in the high-pressure limit up to 2000 K demonstrating similar *A* factors.

Conclusions

We have determined the temperature dependence of the rate constants, k_2 and k_3 for the CH_2OO + CH_3COCH_3 and CH_2OO + CH_3CHO reactions over the temperature range 298-500 K. The results show a decrease in k_2 and k_3 of a factor of 4 over this temperature range. Theoretical analysis suggests that the overall kinetics are determined mainly by the tight 1,3-cycloaddition saddle point. The computed high- and low-pressure rate-coefficients both show negative temperature dependence although the experimentally determined slope is in much better agreement with the low-pressure estimates. Weak pressure dependence is observed for both reactions at 298 K over the pressure range 10 to 50 Torr He. Under our experimental conditions, no pressure effect could be discerned at 444 K. These findings are supported by the theoretical calculations, which predict that the variations of the overall rate coefficients for both reactions are negligible as a function of pressure in the pressure range of interest. Previous work on these systems has shown that organic acids, HCOOH and CH_3COOH are the dominant products for the CH_2OO + CH_3CHO reaction at low pressures.[9,15] HCOOH formation was predicted to be dominant for the CH_2OO + CH_3COCH_3 reaction. The yield of SOZ is relatively small compared to organic acids at

the pressure range studied. Using PI TOF-MS, two product masses were observed; m/z = 89 and m/z = 104 for the reaction of CH_2OO + CH_3COCH_3, which have been tentatively assigned[9] to a daughter ion of methoxymethyl acetate and SOZ, respectively. The relative yield of these products was found to have zero-to-weak pressure dependence at 298 K while the yield of m/z = 89 increases with pressure over the same range. Both of these experimental results are consistent with the previous conclusions of Taatjes et al.[9] regarding the identity of the m/z = 89 species, but there are many unknowns in the chemistry of chemically-activated SOZ, and further exploration of the CH_2OO + CH_3COCH_3 PES would be most helpful.

Associated content

More details on the condition of control experiments and their results, details of the experimental quantification of pressure-dependent product yields, the measured *P*-dependent yield of the m/z = 104 product, additional calculations and a quantitative comparison with the HCHO yield measurements of Stone et al.

Acknowledgements

R.M.I.E. gratefully acknowledges financial support from the Fulbright Commission and Alexandria University. This work was supported by the U.S. Department of Energy, Office of Basic Energy Sciences under the Energy Frontier Research Center for Combustion Science (Grant DESC0001198).

Author Information

Corresponding Author

*E-mail: whgreen@mit.edu

References

1. R. Criegee, G. Wenner, *Justus Liebigs Annalender Chemie*, 1949, **546** (1), 9.

2. L. Vereecken and J. S. Francisco, *Chem. Soc. Rev.*, 2012, **41** (19), 6259.

3. A. R. Cox and S. A. Penkett, Journal of the Chemical Society, *Faraday Trans. 1*, 1972, **68**, 1735.

4. O. Welz, J. D. Savee, D. L. Osborn, S. S. Vasu, C. J. Percival, D. E. Shallcross and C. A. Taatjes, *Science*, 2012, **335**,204.

5. L. Vereecken, H. Harder and A. Novelli, *Phys. Chem. Chem. Phys.*, 2012, **14**, 14682.

6. R. L. Mauldin III, T. Berndt, M. Sipilae, P. Paasonen, T. Petaja, S. Kim T. Kurten, F. Stratmann, V. M. Kerminen and M. Kulmala, *Nature*, 2012, **488**, 193-197.

7. T. R. Lewis, M. Blitz, D. E. Heard, and P. Seakins, *Phys. Chem. Chem. Phys*. 2015, 17, 4859.

8. Z. J. Buras, R. M. I. Elsamra, A.Jalan, J. E. Middaugh, W. H. Green, *J. Phys. Chem. A*, 2014, 118(11), 1997.

9. C. A. Taatjes, O. Welz, A. J. Eskola, J. D. Savee, D. L. Osborn,E. P. F. Lee, J. M. Dyke, D. W. K. Mok, D. E. Shallcross and C. J. Percival, *Phys. Chem. Chem. Phys.*, 2012, **14**, 10391–10400.

10. D. Stone, M. Blitz, L. Daubney, N. U. M. Howes and P. Seakins, *Phys. Chem. Chem.Phys.*, 2014, **16**, 1139.

11. O. Horie, C. Schafer, G. K. Moortgat, *Int. J. Chem. Kinet.*, 1999, **31**, 261.

12. T. Berndt, R. Kaethner, J. Voigtlander, F. Stratmann, M. Pfeifle, P. Reichle, M. Sipila, M. Kulmala and M. Olzmann, *Phys. Chem. Chem. Phys.*, 2015, **17**, 19862 – 19873.

13. P. Aplincourt, M. F. Ruiz-López, *J. Phys. Chem. A*, 2000, **104**, 380-388.

14. P. Aplincourt, M. F. Ruiz-López, *J. Am. Chem. Soc.*, 2000, **122**, 8990-8997.

15. A. Jalan, J. W. Allen, W. H. Green, *Phys. Chem. Chem. Phys.*, 2013, **15**, 16841- 16852.

16. H. Ismail, P. R. Abel, W. H. Green, A. Fahr, L. E. Jusinski, A. M. Knepp, J. Zádor, G. Meloni, T. M. Selby, D. L. Osborn and C. A. Taatjes, *J. Phys. Chem. A*, 2009, **113** (7), 1278-1286.

17. J. E. Middaugh, Ph. D. Thesis, MIT, 2014.

18. S. L. Baughcum and S. R. Leone, *J. Chem. Phys.* 1980, **72** (12), 6531-6545.

19. Z. J. Buras, R. M. I. Elsamra, W. H. Green, *J. Phys. Chem. Lett*. 2014, **5**, 2224-2228.

20. W.-L Ting, Y.-H. Chen, W. Chao, M. C. Smith, J. J.-M. Lin, *Phys. Chem. Chem. Phys.* 2014, **16**, 10438-10443.

21. W.-L. Ting, C.-H. Chang, Y.-F. Lee, H. Matsui, Y.-P. Lee and J. J.-M. Lin, *J. Chem. Phys*., 2014, 141, 104308.

22. R. C. Pun, A. Davey, D. E. Shallcross, C. J. Percival and A. J. Orr-Ewing, *Phys. Chem. Chem. Phys.*, 2015, 17, 3617.

23. D. L. Yang, T. Yu, S. W. Wang and M. C. Lin, *J. Chem. Phys*., 1992, **160**, 307.

24. D. Cremer, J. Gauss, E. Kraka, J. F. Stanton and R. J. Bartlett, *J. Chem. Phys. Lett.*,1993,**209**, 547.

25. M. T. Nguyen, T. L. Nguyen, V. T. Ngan and H. M. T. Nguyen, *J. Chem. Phys. Lett.* 2007, **448**, 183-188.

26. J. C. Traeger, *Int. J. Mass Spectrom. Ion Processes* 1985, **66**, 271-282.

27. J. W. Allen, S. S. Merchant, C. Gao, N. W.-W. Yee, B. A. Buesser, R. H. West and W. H. Green, *RMG-Py version 1.0*, 2013.

28. J. W. Allen, C. F. Goldsmith, W. H. Green, *Phys. Chem. Chem. Phys.*, 2012, **14**, 1131-1155.

29. Y. Georgevskii and S. J. Klippenstein, *J. Chem. Phys.*, 2005, **122**,194103.

30. E. P. F. Lee, D. K. W. Mok, D. E. Shallcross, C. J. Percival, D. L. Osborn, C. A. Taatjes and J. M. Dyke, *Chem. Eur. J.*, 2012, **18**, 12411–12423.

31. E. E. Greenwald, S. W. North, Y. Georgevskii and S. J. Klippenstein, *J. Phys. Chem. A*, 2007, **111**, 5582-5592.

TOC Graphic

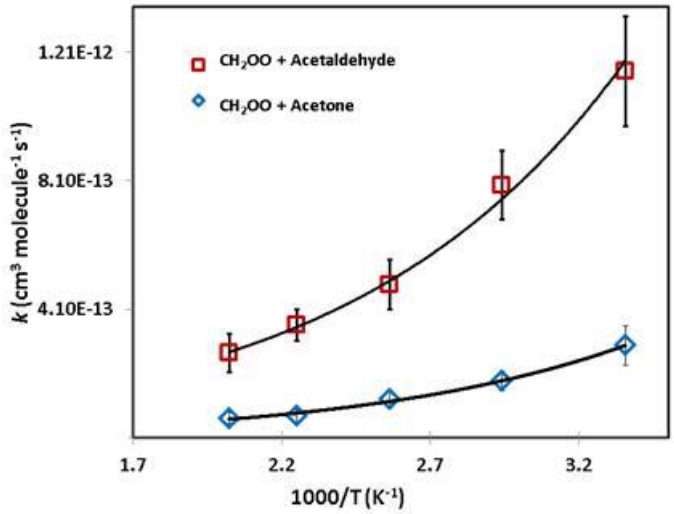

Supporting Information

Temperature and Pressure Dependent Kinetics of $CH_2OO + CH_3COCH_3$ and $CH_2OO + CH_3CHO$: Direct Measurements and Theoretical Analysis

Rehab M. I. Elsamra,[†,‡] Amrit Jalan,[†] Zachary J. Buras,[†] Joshua E. Middaugh,[†] and William H. Green.[†*]

[†] Department of Chemical Engineering, Massachusetts Institute of Technology, 77 Massachusetts Avenue, Cambridge, MA 02139, USA.
[‡] Department of Chemistry, Faculty of Science, Alexandria University, Ibrahimia, 21321, Alexandria, Egypt.

UV Absorption experiments at different T and P:

Table S1 summarizes the conditions of the $CH_2OO + CH_3COCH_3/CH_3CHO$ experiments. In all our experiments $[O_2]$ was kept constant (6.1×10^{16} molecule cm^{-3}), $[CH_3COCH_3]$ was varied from $1.59 \times 10^{14} – 1.35 \times 10^{15}$ molecule cm^{-3} and $[CH_3CHO]$ was varied from $1.59 \times 10^{14} – 1.11 \times 10^{15}$ molecule $cm^{-3.}$ The number of flashes per refresh was 1.21 and the photolysis beam diameter = 1.15 cm.

Table S1: Experimental conditions for *T*- and *P*- dependence UV absorbance experiments

Base case experiments	*T* K	*P* Torr	$[CH_2I_2]^a$ molecule/cm^3	Photolysis power mJ/ pulse
T-dependence	(298 ± 1.3) to (494 ± 5)	25	1.35×10^{14}	50
P- dependence	(298 ± 1.3) and (444 ± 3)	4 - 50	1.35×10^{14}	50
Control experiments				
Max. Photolysis energy	(298 ± 1.3) and (494 ± 5)	25	1.35×10^{14}	100
double $[CH_2I_2]$	(298 ± 1.3) and (494 ± 5)	25	2.44×10^{14}	50

[a] $[CH_2I_2]$ was estimated by using the vapor pressure of CH_2I_2 at 298 K[1]

Two absorbance-control experiments were conducted at 298 and 494 K at constant pressure of 25 Torr, one with double the base case precursor concentration ([CH_2I_2]) and the other at maximum photolysis energy (100mJ/pulse). These control experiments were performed to confirm that no interfering secondary chemistry was being observed under the base case conditions. Traces were also recorded in the absence of O_2 or CH_2I_2 at every temperature to ensure that no CH_2OO radicals are formed except under the normal reactor conditions (i.e., with both CH_2I_2 and O_2 gases present) and/or that no other species are contributing to the 375 nm absorbance signal. Results of control experiments are shown in Fig. S1.

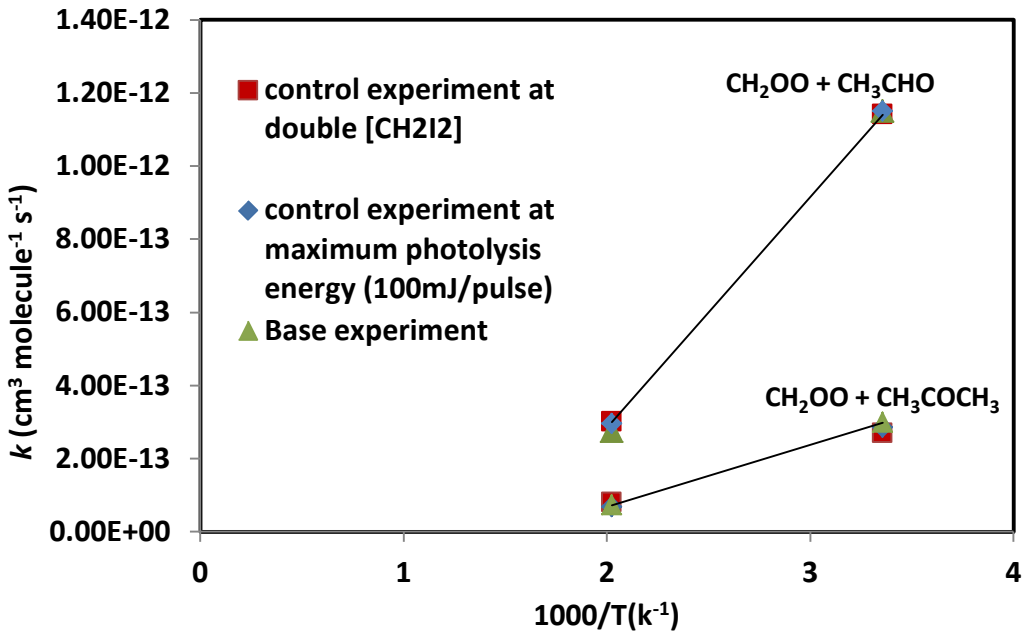

Figure S1. Control experiments at 298 K and 494 K together with the base experiments for CH_2OO + CH_3CHO (top points) and CH_2OO + CH_3COCH_3 (bottom points).

Figure S1 shows example of the control experiments carried out at the double concentration of CH_2I_2 and at maximum laser photolysis energy. As seen in the figure, the control results are consistent with the base condition ([CH_2I_2] = 1.35×10^{14} molecules cm^{-3} and 50 mJ/pulse), implying that the effect of laser energy and precursor concentration on the measured rate coefficients is negligible.

CH_2OO + CH_3COCH_3 MS Control Experiments

In addition to $\frac{m}{z} = 46$ amu (the mass of the simplest CI, CH_2OO), we observed four other transient species in our $\frac{m}{z}$ range of interest (0-104 amu) in the "Base Case" mass spectrometry (MS) experiment: $\frac{m}{z} = 31, 73, 89$ and 104 amu. Transient behavior was not discernible at $\frac{m}{z} = 15$ due to overlap with a CH_3COCH_3 fragment. This Base Case refers to the conditions where CH_2OO + CH_3COCH_3 is occurring and there is also calibration mixture (cal mix) present in the reactor to act as an internal standard (Base Case = CH_2I_2 + O_2 + CH_3COCH_3 + cal mix + 355 nm photolysis). Control MS experiments were conducted without CH_3COCH_3, without O_2 and without cal mix to identify which of these transient species are possible products of CH_2OO + CH_3COCH_3. The maximum signal of transient species i, $S_{i,max}$, was normalized by the initial amount of CH_2I present, $[\mathrm{CH_2I}]_0$ (obtained from simultaneously recorded I Atom Absorbance), and the average internal standard (benzene) signal during that experiment, $\bar{S}_{benzene}$:

$$\hat{S}_{i,max} = S_{i,max}/([\mathrm{CH_2I}]_0 \bar{S}_{benzene})$$

Performing this normalization removes the effect of varying CH_2I concentration and MS signal response from experiment to experiment. The ratio of $\hat{S}_{i,max}$, for a given control experiment with the base case experiment was then taken:

$$\frac{\left(\hat{S}_{i,max}\right)_{Control}}{\left(\hat{S}_{i,max}\right)_{Base\ Case}} = \frac{[i]_{max,Control}}{[i]_{max,Base\ Case}}$$

As shown, this ratio is indicative of how much the concentration of transient species, i, changed going from the Base Case to the control experiment. Table S2 summarizes the results of this analysis for the three control experiments mentioned above. Note that for the "No Cal Mix" control, $\bar{S}_{benzene} = 0$, so for this experiment we had no internal standard to use and we assumed that the signal response of the MS was the same for this control experiment as for the base case. We believe this is a good assumption because the Base Case and "No Cal Mix" experiments were done back-to-back for this reason, and because the Cal Mix was present in such low concentration ($\sim 10^{11}$ molecules cm^{-3} compared to $\sim 10^{17}$ molecules cm^{-3} total at the pressure of these experiments, 10 Torr) that the MS signal response should not be affected by removing it anyway.

Table S2. Results of MS control experiments for CH_2OO + CH_3COCH_3. $\boldsymbol{T = 298\ K}$ and $\boldsymbol{P = 10\ Torr}$. For Base Case experiment: [CH_3COCH_3]= 1.24×10^{15} molecule cm^{-3}, [CH_2I_2] = 2.44×10^{14}, [O_2] = 6×10^{16} molecule cm^{-3} and [Cal Mix Species] = 1.6×10^{11} molecule cm^{-3}. Each Control experiment was conducted under identical conditions as the Base Case experiment, except for the one change noted.

	$\frac{[i]_{max,control}}{[i]_{max,Base\ Case}}$ for $\frac{m}{z}$ =			
MS Control Experiment	31 amu	73 amu	89 amu	104 amu
No Acetone	1.0 ± 0.4	1.3 ± 0.5	0	0
No O_2	1.1 ± 0.4	1.1 ± 0.4	0	0
No Cal Mix.	0.17 ± 0.06	1.7 ± 0.6	1.0 ± 0.4	1.1 ± 0.7

There are several important things to note about these results. First, the species at $\frac{m}{z} = 89$ and 104 amu only appear when both acetone and O_2 are present and their maximum concentrations are not affected by the presence of Cal Mix. Therefore, we conclude that these two species are products of CH_2OO + CH_3COCH_3, consistent with what Taatjes et al. have observed.[2] Second, the species at $\frac{m}{z} = 31$ and 73 amu are present at the same maximum concentration regardless of whether acetone or O_2 are present. Therefore $\frac{m}{z} = 31$ and 73 amu cannot be products of CH_2OO + CH_3COCH_3. Finally, the maximum concentration of $\frac{m}{z} = 31$ decreases substantially without Cal Mix present, indicating that how much $\frac{m}{z} = 31$ is being formed depends on one of the Cal Mix species being present. At the same time that the maximum concentration of $\frac{m}{z} = 31$ decreases with no Cal Mix, the maximum concentration of $\frac{m}{z} = 73$ increases, likely because whatever channels are producing $\frac{m}{z} = 31$ and $\frac{m}{z} = 73$ amu are competing for CH_2I. Therefore, if the rate for the $\frac{m}{z} = 31$ producing channel decrease, there is more CH_2I available to form $\frac{m}{z} = 73$ amu. We think that $\frac{m}{z} = 73$ is produced by a side reaction involving a contaminant in our reactor, which previous to the current Criegee Intermediate studies has been used for studies on the vinyl and allyl radical.

Quantifying Pressure-Dependent Product Yields for CH_2OO + CH_3COCH_3

The kinetic model from the main text is reproduced here for reference.

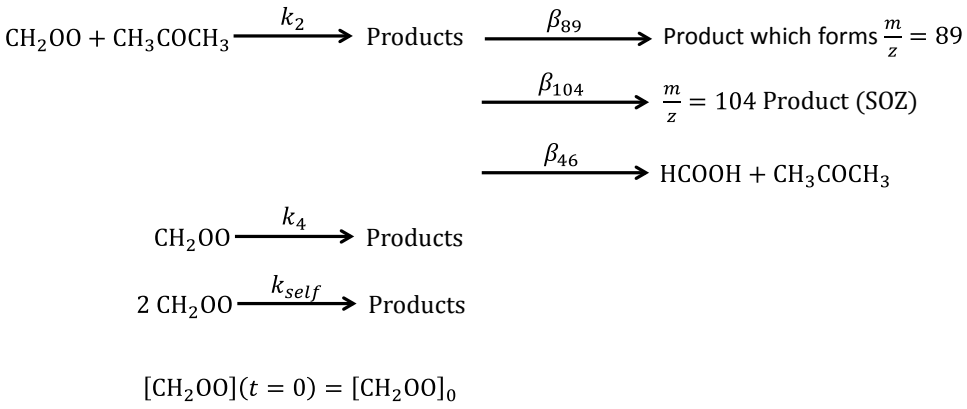

Scheme 1. General kinetic model for CH_2OO + CH_3COCH_3

Assuming that CH_3COCH_3 is present in excess, the analytical expressions for $[CH_2OO](t)$ and the steady state concentration of the CH_2OO + Acetone products, $[Products]_{CI+Acetone}\ (t \to \infty)$, based on the kinetic model above are the following:

$$[CH_2OO](t) = \frac{(k_2[CH_3COCH_3]+k_4)[CH_2OO]_0}{(k_2[CH_3COCH_3]+k_4+2k_{self}[CH_2OO]_0)e^{(k_2[CH_3COCH_3]+k_4)t}-2k_{self}[CH_2OO]_0}$$

$$[\text{Products}_{(CI+Acetone)}](t \to \infty) = \frac{k_2[CH_3COCH_3]}{2k_{self}} \ln\left(\frac{k_2[CH_3COCH_3]+k_4+2k_{self}[CH_2OO]_0}{k_2[CH_3COCH_3]+k_4}\right)$$

It is clear that the time dependence of CH_2OO and the steady state concentration of the products of its reaction with CH_3COCH_3 depend on many parameters: $[CH_2OO]_0$, k_2, k_{self} and k_4. k_2 is known from the UV absorbance experiments also reported in this work. The experiments to quantify the other parameters are discussed below.

The initial concentration of CH_2OO, $[CH_2OO]_0$, in the above equation can be quantified from transient I atom absorbance assuming that $[CH_2I]_0 = [I]_0$. A narrow linewidth low-noise continuous-wave diode laser was used to generate an infrared beam tuned to the ($F = 3\ ^2P_{1/2} \leftarrow F = 4\ ^2P_{3/2}$) I atom atomic transition.[3] The infrared path lengths for I atom absorption were in the range of $50 - 70$ cm. Both ultraviolet

and single-pass infrared absorbance traces were averaged over 500 acquisitions and recorded simultaneously.

We have previously shown that the I atom absorbance, A_I, may be fit adequately to the following equations.[4]

$$[\mathrm{I}](t) = \frac{[\mathrm{CH_2I}]_0}{k_1[\mathrm{O_2}] - k_5}\left([(1+\alpha)k_1[\mathrm{O_2}] - k_5]e^{-k_5 t} - \alpha k_1[\mathrm{O_2}]e^{-k_1[\mathrm{O_2}]t}\right)$$

$$A_I(t) = \sigma_{\mathrm{I}}(\lambda = 1315.246\ \mathrm{nm})\, l_I [\mathrm{I}](t)$$

Where α is the branching fraction of $CH_2I + O_2$ to CH_2OO, k_1 is the total rate of that reaction, k_5 is the first order loss rate of I atom due to various processes, $\sigma_I(\lambda)$ is the known absorption cross section of I atom for a given hyperfine transition and l_I is the measured path length of the I atom laser. In these equations, α and k_1 are global fit parameters and k_5 and $[\mathrm{CH_2I}]_0$ are local fit parameter (i.e. a different value of each is fit for every trace). The quantity $\alpha[\mathrm{CH_2I}]_0$ is equal to $[\mathrm{CH_2OO}]_0$. A representative fit to an I atom trace is shown in Fig. S2.

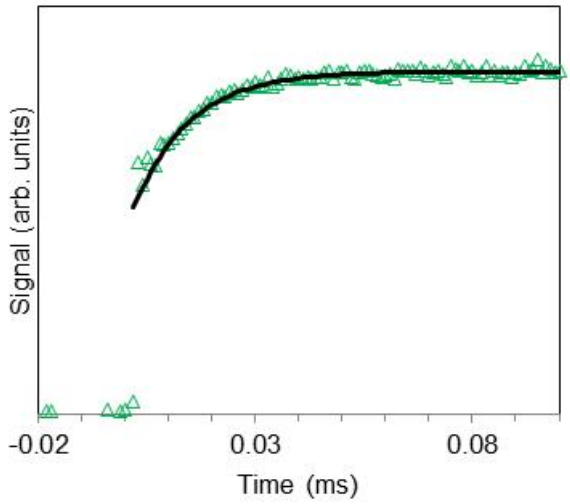

Figure S2. Representative I atom trace at 298 K, 10 Torr and $[\mathbf{O_2}] = \mathbf{6.0 \times 10^{16}\ cm^{-3}}$ with model fit to extract value of $[\mathbf{CH_2OO}]_\mathbf{0}$. Only every 100th point is shown.

The growth in I Atom absorbance shown in Fig. S2, A_I, corresponds to the sum of the initial photolytic production of I, and the production of I by the reaction $\mathrm{CH_2I + O_2 \rightarrow CH_2OO + I}$ with rate $k_1 (= 1.4 \pm 0.1 \times 10^{-12}\ \mathrm{cm^3\ molecule^{-1}\ s^{-1}})$.[4,5] The amount of I Atom produced by the second process, $[\mathrm{I}]_0$, can be captured and is equal to the amount of $[\mathrm{CH_2OO}]$ formed.

The equation for $[Products]_{Cl+Acetone}$ $(t \to \infty)$, also depends on k_{self} and k_4. Until recently, k_{self} had not previously been experimentally measured, although Vereecken et al.[6] had predicted a value of $k_{self} \approx 3.8 \times 10^{-11}\text{cm}^3\text{molecule}^{-1}\text{cm}^{-1}$ using quantum calculations and TST. Very recently and just prior to the current work, our group was successfully able to experimentally measure k_{self} using UV absorption.[7] We measured $k_{self} = 6.2 \pm 2.2 \times 10^{-11}\text{cm}^3\text{molecule}^{-1}\text{cm}^{-1}$, in good agreement with Vereecken et al. and later experimental measurements by Ting et al.[8] and Chhantyal-Pun et al.[9] We used this value of k_{self} in all calculations here.

The value of k_4, which includes diffusion out of the sampling volume, could change significantly if the experimental apparatus is modified. This study was conducted over the course of a few days, however, during which time the reactor was kept as static as possible. Therefore, for a given pressure and temperature, we expect this value to be roughly the same for all of the results reported here.

In order to obtain values for k_4 at 10, 25 and 50 Torr (temperature is always 298 K), the decay of $\frac{m}{z} = 46$ measured by TOF-MS, $S_{46}(t)$, was recorded under conditions where CH_2OO is formed (ie, CH_2I_2 + O_2 + 355 nm photolysis) both with and without CH_3COCH_3. $S_{46}(t)$ was then normalized and fit to the expression for $\frac{[\text{CH}_2\text{OO}](t)}{[\text{CH}_2\text{OO}]_0}$ above. k_4 was used as fit parameter for traces taken at the same pressure while k_2 and k_{self} were fixed to the values measured with UV absorbance earlier. Representative fits to normalized $S_{46}(t)$ with and without acetone and the fitted values obtained for k_4 are given in Fig. S3 and Table S3, respectively.

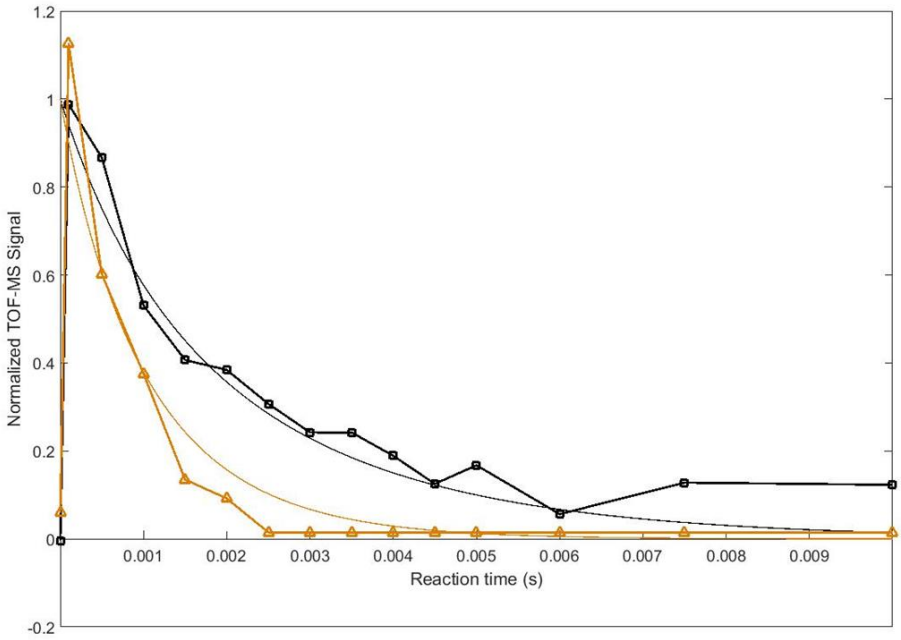

Figure S3. Representative normalized decay of $\frac{m}{z} = \mathbf{46}$ measured by TOF-MS at 298 K, 50 Torr, $[\mathbf{O_2}] = \mathbf{6.0 \times 10^{16} cm^{-3}}$ and $[\mathbf{CH_3COCH_3}] = \mathbf{0}$ (black squares) and $\mathbf{1.24 \times 10^{15}\ cm^{-3}}$ (orange triangles). Thin lines are fits to the kinetic model given in Scheme 1.

Table S3. Values obtained for $\boldsymbol{k_4}$ at 298 K and different pressures.

Pressure (Torr)	$\boldsymbol{k_4}$(s^{-1})
10	**230**
25	**470**
50	**320**

With values of k_2, k_{self} and k_4 known at 10, 25 and 50 Torr, it is possible to calculate $[\mathrm{Products_{CI+Acetone}}](t \to \infty)$ at those conditions for a given $[CH_2OO]_0$ and $[CH_3COCH_3]$.

The steady state concentrations of the $\frac{m}{z} = 89$ and 104 amu product species are related to $[\mathrm{Products_{(CI+Acetone)}}](t \to \infty)$ through their respective branching fractions, β_i, by the following equations.

$$\left[\frac{m}{z} = 89 \text{ amu}\right](t \to \infty) = \beta_{89}\left[\text{ Products}_{(\text{CI+Acetone})}\right](t \to \infty)$$

$$\left[\frac{m}{z} = 104 \text{ amu}\right](t \to \infty) = \beta_{104}[\text{Products}_{\text{CI+Acetone }}](t \to \infty)$$

The general relationship between the PI TOF-MS signal due to a species i, S_i, (measured as integrated peak area) and its concentration is the following.

$$S_i = FR_i\sigma_i(E)[i]$$

Where F is the instrument response factor, R_i is the mass discrimination factor and $\sigma_i(E)$ is the photoionization cross-section of species i at energy E. Accordingly, the steady-state PI TOF-MS signals for $\frac{m}{z} = 89$ amu and $\frac{m}{z} = 104$ amu can be expressed as follows.

$$S_{89}(t \to \infty) = FR_{89}\sigma_{89}(E = 10.5 \text{ eV})\left[\frac{m}{z} = 89 \text{ amu}\right] \quad (t \to \infty)$$

$$S_{104}(t \to \infty) = FR_{104}\sigma_{104}(E = 10.5 \text{ eV})\left[\frac{m}{z} = 104 \text{ amu}\right] \quad (t \to \infty)$$

Or

$$S_{89}(t \to \infty) = FR_{89}\sigma_{89}(E = 10.5 \text{ eV})\beta_{89}\left[\text{Products}_{(\text{CI+Acetone })}\right](t \to \infty)$$

$$S_{104}(t \to \infty) = FR_{104}\sigma_{104}(E = 10.5 \text{ eV})\beta_{104}\left[\text{Products}_{(\text{CI+Acetone })}\right](t \to \infty)$$

In all of our PI TOF-MS experiments, a small amount of a gas mixture with known composition was simultaneously flowed in the reactor to act as an internal standard. The concentrations of calibration mixture species are small so as not to interfere with the chemistry (10^{11} cm^{-3}) and known to within 15% based on the reactor conditions. The mixture contains 101 ppm of each of the following species: methylamine (31 amu), propene (42 amu), 1,3-butadiene (54 amu), propanol (60 amu), furan (68 amu), benzene (78 amu), cyclohexane (84 amu), toluene (92 amu) and heptane (100 amu).

Taking the ratio of $S_{89}(t \to \infty)$ or $S_{104}(t \to \infty)$, to the average PI TOF-MS signal from any of the calibration mixture species, $\bar{S}_{calmix,j}$, results in the following.

$$\frac{S_{89}(t \to \infty)}{\bar{S}_{calmix,j}} = \frac{FR_{89}\sigma_{89}(E = 10.5 \text{ eV})\beta_{89}\left[\text{Products}_{(\text{CI+Acetone })}\right](t \to \infty)}{FR_{calmix,j}\sigma_{calmix,j}(E = 10.5 \text{ eV})[calmix,j]}$$

$$\frac{S_{104}(t \to \infty)}{\bar{S}_{calmix,j}} = \frac{FR_{104}\sigma_{104}(E = 10.5 \text{ eV})\beta_{104}\left[\text{Products}_{(\text{CI+Acetone })}\right](t \to \infty)}{FR_{calmix,j}\sigma_{calmix,j}(E = 10.5 \text{ eV})[calmix,j]}$$

F cancels out because it is a constant. For our apparatus we have found the mass discrimination factor to have very weak or no dependence on mass. Therefore the ratio of R values also becomes one.

$$\frac{S_{89}(t\to\infty)}{\bar{S}_{calmix,j}} = \beta_{89}\frac{\sigma_{89}(E=10.5\text{ eV})}{\sigma_{calmix,j}(E=10.5\text{ eV})}\frac{[\text{Products}_{(\text{CI+Acetone})}](t\to\infty)}{[calmix,j]}$$

$$\frac{S_{104}(t\to\infty)}{\bar{S}_{calmix,j}} = \beta_{104}\frac{\sigma_{104}(E=10.5\text{ eV})}{\sigma_{calmix,j}(E=10.5\text{ eV})}\frac{[\text{Products}_{(\text{CI+Acetone})}](t\to\infty)}{[calmix,j]}$$

These equations can be rearranged for, $\sigma_{89}\beta_{89}$ and $\sigma_{104}\beta_{104}$.

$$\sigma_{89}\beta_{89} = \sigma_{calmix,j}(E=10.5\text{ eV})\frac{S_{89}(t\to\infty)}{\bar{S}_{calmix,j}}\frac{[calmix,i]}{[\text{Products}_{(\text{CI+Acetone})}](t\to\infty)}$$

$$\sigma_{104}\beta_{104} = \sigma_{calmix,j}(E=10.5\text{ eV})\frac{S_{104}(t\to\infty)}{\bar{S}_{calmix,j}}\frac{[calmix,i]}{[\text{Products}_{(\text{CI+Acetone})}](t\to\infty)}$$

The quantity $\sigma_i\beta_i$, where $i = 89$ or 104, cannot be separated because σ_i is not known. If, however, we assume that σ_i is independent of pressure, then we can ratio the measured value of $\sigma_i\beta_i$ at one pressure, $(\sigma_i\beta_i)_{\text{P1}}$, to another pressure, $(\sigma_i\beta_i)_{\text{P2}}$ and cancel out the σ_i values.

$$\frac{(\sigma_i\beta_i)_{\text{P1}}}{(\sigma_i\beta_i)_{\text{P2}}} = \frac{(\beta_i)_{\text{P1}}}{(\beta_i)_{\text{P2}}}$$

Furthermore, if we assume that $\sigma_{calmix,j}$ and σ_i are pressure independent:

$$\frac{(\beta_i)_{\text{P1}}}{(\beta_i)_{\text{P2}}} = \frac{\left(\frac{S_i(t\to\infty)}{\bar{S}_{calmix,i}}\frac{[calmix,i]}{[\text{Products}_{(\text{CI+Acetone})}](t\to\infty)}\right)_{\text{P1}}}{\left(\frac{S_i(t\to\infty)}{\bar{S}_{calmix,i}}\frac{[calmix,i]}{[\text{Products}_{(\text{CI+Acetone})}](t\to\infty)}\right)_{\text{P2}}}$$

This equation was given in the main text. In this manner, the relative pressure dependent yield of both $\frac{m}{z} = 89$ and $\frac{m}{z} = 104$ can be computed.

Note that, of the nine species present in the calibration mix, only benzene is a suitable internal standard. Of the other eight, propene and 1,3-butadiene overlap with acetone fragment signals in the mass spectrum, methylamine and propanol are not thermally stable, furan and heptane have low signal (relatively small cross sections), and the

concentrations of toluene and cyclohexane have decreased below 101 ppm over the lifetime of the gas cylinder. The stable benzene signal used as an internal standard is shown in Fig. S4.

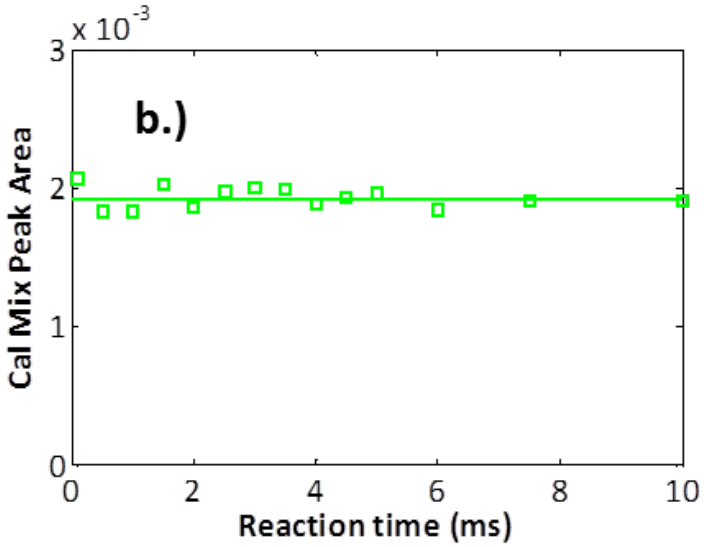

Figure S4. TOF-MS signal of the internal benzene standard at 298 K, 10 Torr, $[\mathbf{O_2}] = \mathbf{5.95 \times 10^{16} cm^{-3}}$ and $[\mathbf{CH_3COCH_3}] = \mathbf{1.24 \times 10^{15} cm^{-3}}$ recorded simultaneously as the product signals shown in Fig. 6. The line is an average values of the stable benzene signal, $\overline{S}_{calmix,benzene}$.

Figure S5 shows the measured values of $\frac{(\beta_i)_{P1}}{(\beta_i)_{P2}}$ for $\frac{m}{z} = 104$ amu as a function of pressure. The TOF-MS signal for this species was too low to discern a trend with respect to pressure (S_{104} has low signal/noise ratio).

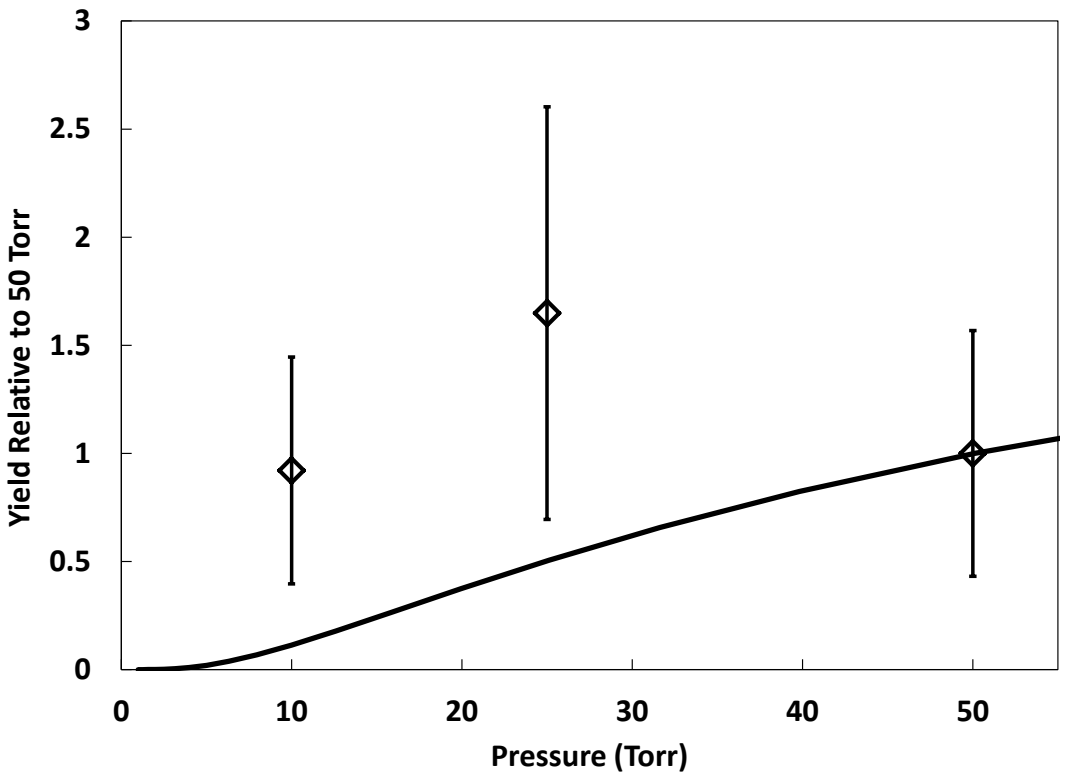

Figure S5. Relative yield of $\frac{m}{z} = 104$ amu product from CH_2OO + CH_3COCH_3 normalized to the 50 Torr measurement $\left(\frac{(\beta_{104})_{\mathrm{P=X\ Torr}}}{(\beta_{104})_{\mathrm{P=50\ Torr}}}\right)$ at 298 K (markers) compared to predicted relative yield of SOZ at the same conditions from Jalan et al.[10] (line). The error bar on the 50 torr point indicates the uncertainty in that measurement (which is used to normalize the other two points.)

Theoretical Calculations

Fig. S6 shows the lack of sensitivity to $k_{outer}^{P=\infty}$ exhibited by $k_{observable}^{P=0}$ and $k_{observable}^{P=\infty}$. Fig. S7 shows the logarithm of the various contributions to the ratio of inner TS to reactant partition functions, $\frac{Q_{TS,inner}}{Q_{reactants}}$, in the expression for $k_{TST}(T)$ below:

$$k_{TST}(\mathrm{T}) = \frac{k_B T}{h}\left(\frac{Q_{TS,inner}}{Q_{reactants}}\right) \times \exp\left(-\frac{\left[E_0^{TS,inner} - E_0^{reactants}\right]}{RT}\right)$$

$$\log_{10}\left(\frac{Q_{TS,inner}}{Q_{reactants}}\right) = \log_{10}\left(\frac{Q_{TS,inner}}{Q_{reactants}}\right)_{rot} + \log_{10}\left(\frac{Q_{TS,inner}}{Q_{reactants}}\right)_{vib} + \log_{10}\left(\frac{Q_{TS,inner}}{Q_{reactants}}\right)_{trans} + \log_{10}\left(\frac{Q_{TS,inner}}{Q_{reactants}}\right)_{hindered\ rotor} + \log_{10}\left(\frac{Q_{TS,inner}}{Q_{reactants}}\right)_{optical\ isomers}$$

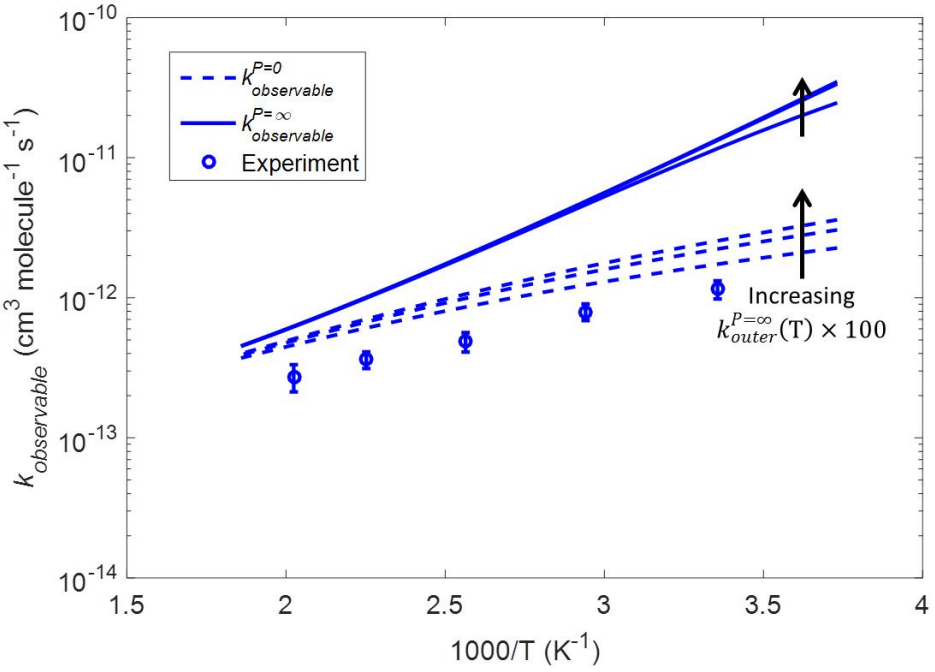

(a)

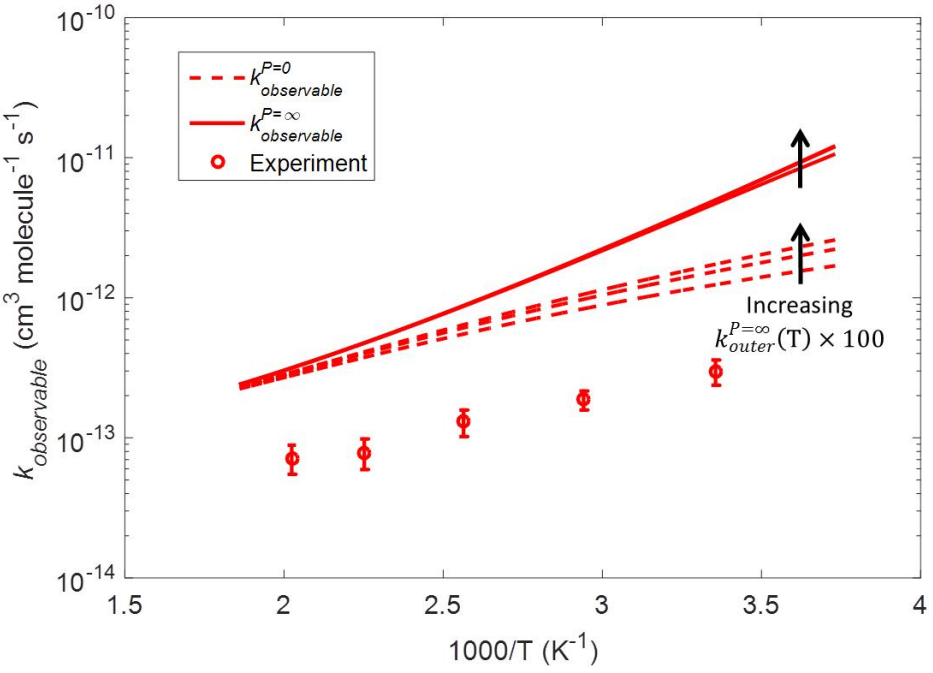

(b)

Figure S6. Predicted T-dependence of $k^{P=0}_{observable}$ and $k^{P=\infty}_{observable}$ over a range of $k^{P=\infty}_{outer}$ for (a) CH_2OO + CH_3CHO and (b) CH_2OO + CH_3COCH_3

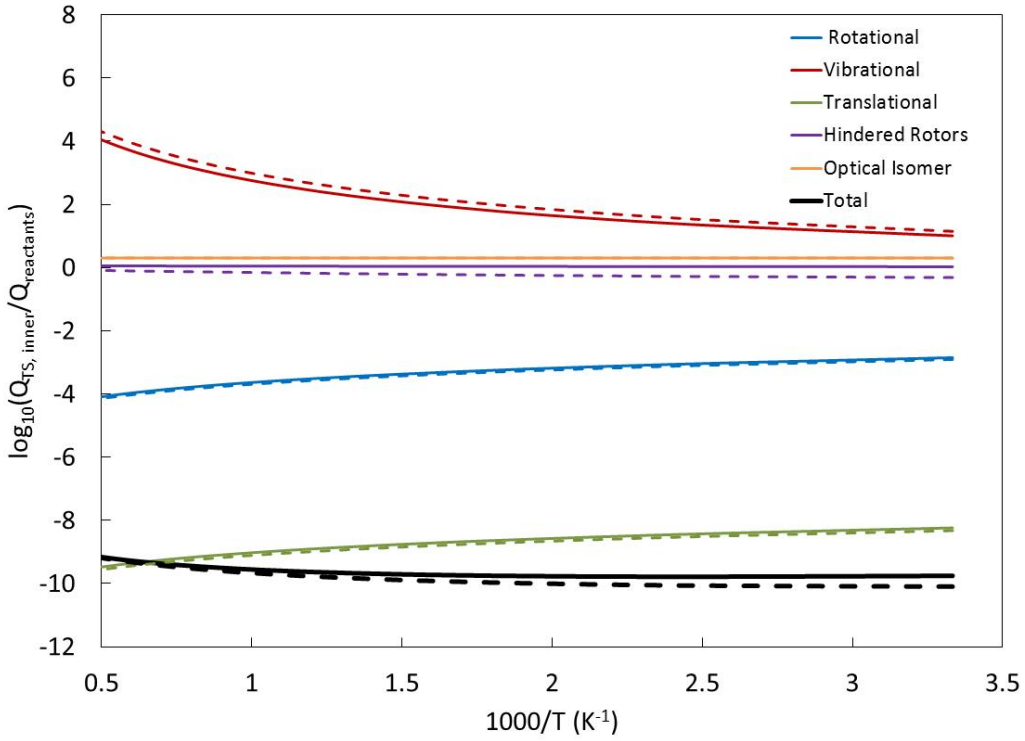

Figure S7. Different contributions to the ratio $Q_{TS,inner}/Q_{reactants}$ in the TST expression for the high-P limit *k*, demonstrating the dominance of the vibrational term at higher temperatures. Solid lines are for CH_2OO + CH_3CHO and dashed lines are for CH_2OO + CH_3COCH_3.

Comparison of Predictions with HCHO Yield Measurements of Stone et al.

Using HCHO laser-induced fluorescence (LIF), Stone et al. quantified yields of HCHO from CH_2OO + CH_3CHO at 295 K in 25 to 300 Torr of mostly N_2 bath gas.[11] They observed that the yield decreased significantly with increasing pressure and by fitting their data to a Stern-Volmer equation they were able to estimate an HCHO yield of 88% at 4 Torr and 4% at 730 Torr (in N_2). At first glance, these measurements seem to be inconsistent with our own predictions of the CH_2OO + CH_3CHO product distribution, wherein the low-pressure HCHO yield at room temperature is ~25%, and the remaining ~75% is attributable to HCOOH + CH_3CHO (see Fig. 10 of main text and Fig. S8a below). However, this discrepancy can be explained by uncertainties in both the measurements of Stone et al. and our predictions.

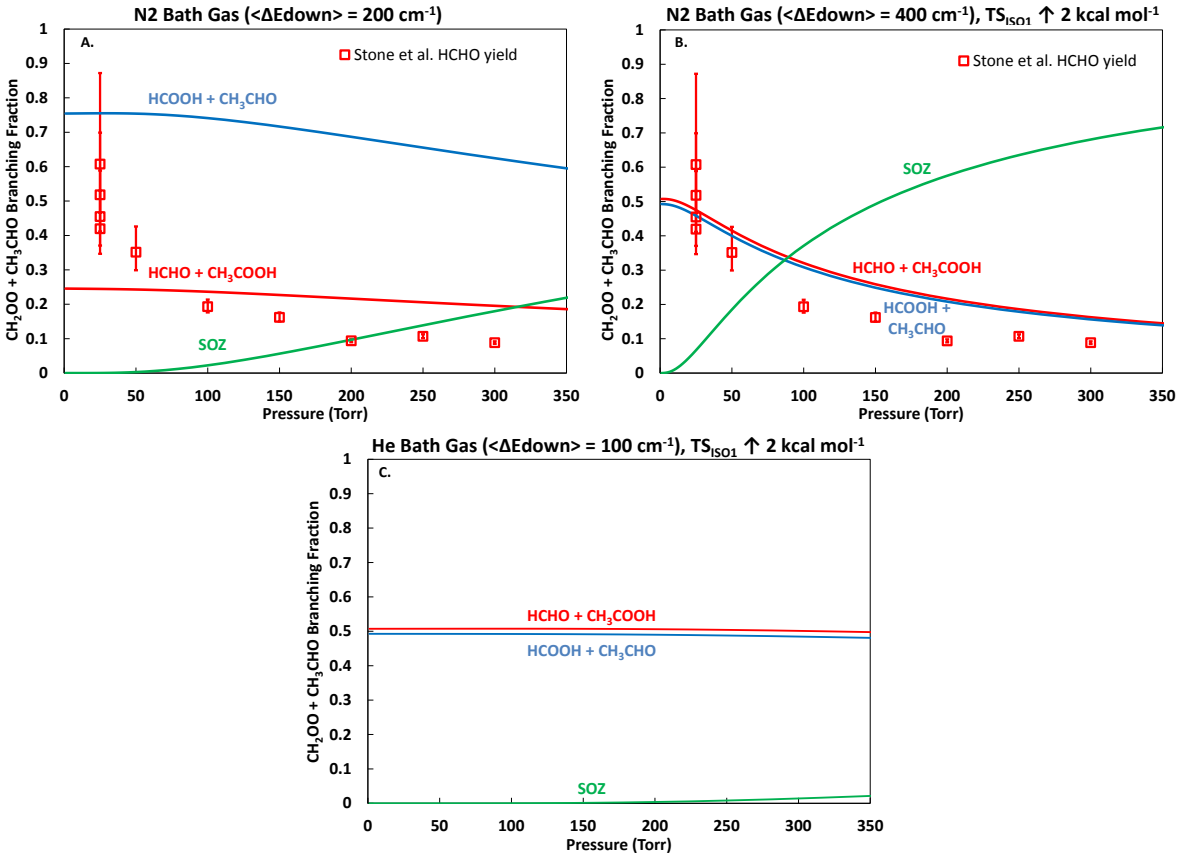

Figure S8. Comparison between HCHO yield measured by Stone et al.[11], and our predictions using the methodology of Jalan et al.[10] with the modifications indicated.

First, in order to obtain the estimates of the HCHO yield above, Stone et al. forced the intercept of their Stern-Volmer plot to equal 1.0, which is tantamount to assuming that in the low-P limit, HCHO is the only product. The authors report that without this assumption, the intercept of the fit is 1.19 ± 0.39, which corresponds to low-pressure HCHO yields in the range of 63-100%. The remainder of the yield can be attributed to the HCOOH + CH_3CHO

product channel, consistent with our predictions and also with the PI TOF-MS measurements of Taatjes et al., where HCHO, CH_3COOH and HCOOH were all observed as products of CH_2OO + CH_3CHO in 4 Torr He.[2]

Second, as demonstrated by Jalan et al., the predicted product branching is quite sensitive to certain transition state energies, as well as the energy transfer model.[10] It was previously shown that the yield of HCHO versus HCOOH is predominantly controlled by the energies of the transition states labelled TS_{ISO1} and TS_{ISO2}, which are only separated by 1.6 kcal mol^{-1}. For the purpose of quantitative comparison with Stone et al., we have increased TS_{ISO1} until our low-pressure predictions are in good agreement with their 25 Torr measurements (Fig. S8b). An increase of 2 kcal mol^{-1} was necessary, which is reasonable given the level of theory used (RCCSD(T)-F12a/VTZ-F12//B3LYP/MG3S) and also considering that in reality it is the combined uncertainty of TS_{ISO1} and TS_{ISO2} (as well as TS_{D3} possibly) that leads to the observed discrepancy.

In order to capture the pressure dependence of the yield measured by Stone et al., we also increased $< \Delta E_{down} >$ for an N_2 bath gas from 200 cm^{-1} to 400 cm^{-1} (Fig. S8b). Although Jalan et al. used the former value for their original predictions in an N_2 bath gas (taken from an *ab initio* study of monomethylhydrazine, CH_3NHNH_2, decomposition in N_2[12]), the latter value also has precedence in the literature (toluene in N_2, for example[13]). Even with this large adjustment, however, our predicted decrease in HCHO yield with pressure is not as steep as Stone et al.'s measurement. This might be explained by underestimated uncertainty in the higher-pressure measurements of Stone et al., where the presence of CH_2IOO complicates their analysis. Furthermore, the scatter in the data at the lowest pressure (25 Torr) suggests that the real uncertainty in the yield at a given pressure is larger than what is indicated by the error bars on an individual measurement.

Finally, as a consistency check, we calculated the product branching at our experimental conditions (4-100 Torr He bath gas) using the modified PES (TS_{ISO1} increased by 2 kcal mol^{-1}). Fig. S8c shows that even up to 100 Torr the branching to SOZ is negligible, consistent with the lack of SOZ observed by either us or Taatjes et al. at these conditions.

References

1.CRC Handbook of Chemistry and Physics. In Physical Constants of Organic Compounds [Online] 89 ed.; Lide, D. R., Ed. CRC Press/Taylor and Francis: Boca Raton, FL, 2009.

2. C. A. Taatjes, O. Welz, A. J. Eskola, J. D. Savee, D. L. Osborn,E. P. F. Lee, J. M. Dyke, D. W. K. Mok, D. E. Shallcross and C. J. Percival, *Phys. Chem. Chem. Phys.*, 2012, **14**, 10391–10400.

3. S. L. Baughcum and S. R. Leone, *J. Chem. Phys.* 1980, **72** (12), 6531-6545.

4. Z. J. Buras, R. M. I. Elsamra, A. Jalan, J. E. Middaugh, W. H. Green, *J. Phys. Chem. A*, 2014, **118**, 1997- 2006.

5. A. J. Eskola, D. Wojcik-Pastuszka, E. Ratajczak, R. S. Timonen, *Phys. Chem. Chem. Phys.* 2006, ***8***, 1416-1424.

6. L. Vereecken, H. Harder, A. Novelli, *Phys. Chem. Chem. Phys.* 2014, 4039-4049.

7. Z. J. Buras, R. M. I. Elsamra, W. H. Green, *J. Phys. Chem. Lett*. 2014, **5**, 2224-2228.

8. W.-L. Ting, C-H. Chang, Y.-F. Lee, H. Matsui, Y.-P. Lee, J. J.-M. Lee, *J. Chem. Phys.* 2014, **141**.

9. R. Chhantyal-Pun, A. Davey, D. E. Shallcross, C. J. Percival, A. J. Orr-Ewing, *Phys. Chem. Chen. Phys.* 2015, **17**, 3617-3626.

10. A. Jalan, J. W. Allen, W. H. Green, *Phys. Chem. Chem. Phys.*, 2013, **15**, 16841- 16852.

11. D. Stone, M. Blitz, L. Daubney, N. U. M. Howes, P. Seakins, *Phys. Chem. Chem. Phys.* 2014, **16**, 1139-1149.

12. P. Zhang, S. J. Klippenstein, H. Sun, C. K. Law, *Proc. Comb. Inst.* 2011, **33**, 425-532.

13. J. A. Miller and S.J. Klippenstein, *J. Phys. Chem. A.* 2003, **107**, 7783-7799.